FEASIBILITY AND ANALYSIS OF A HYBRID SPACESUIT ARCHITECTURE FOR PLANETARY SURFACE EXPLORATION

by

ROGER HUERTA I LLUCH

B.S. Biomedical Engineering, Universitat de Barcelona, 2017

A thesis submitted to the

Faculty of the Graduate School of the

University of Colorado in partial fulfillment

of the requirement for the degree of

Master of Science

Department of Aerospace Engineering Sciences

focus on Bioastronautics

2019

This thesis entitled:
Feasibility and Analysis of a Hybrid Spacesuit Architecture for
Planetary Surface Exploration
written by Roger Huerta i Lluch
has been approved for the Department of Aerospace Engineering Sciences

_____
Allison P. Anderson

_____
Torin P. Clark

_____
David Klaus

Date_____

The final copy of this thesis has been examined by the signatories, and we find that both the content and the form meet acceptable presentation standards of scholarly work in the above mentioned discipline.

Abstract

Huerta i Lluch, Roger (M.Sc., Aerospace Engineering Sciences – Bioastronautics)

Feasibility and Analysis of a Hybrid Spacesuit Architecture for Planetary Surface Exploration.

Thesis directed by Assistant Professor Allison P. Anderson.

This Thesis presents a novel hybrid spacesuit architecture concept to enable planetary exploration by combining mechanical counterpressure (MCP) with gas-pressurization (GP). This conceptual design has the potential to offer a quantifiable increase in mobility, increases in safety through pressure layer redundancy, and decreased pre-breathe time to improve operational efficiency. The Thesis performs an engineering study on the concept. First, to assess the feasibility and benefit of implementing two separate pressure layers in the spacesuit, a trade analysis of the design space was performed by numerically modelling different spacesuit-related parameters. The analysis is done considering the combined system performance across different levels of total pressure and the degree of contribution of each system (MCP-GP). Then, the GP layer of the Hybrid Spacesuit concept is evaluated by testing the dexterity capabilities of gas-pressurized elements not intended for space use. Finally, the Thesis proceeds to develop relevant tools that can help on the development of MCP spacegloves, intended to be integrated into the Hybrid Spacesuit. These tools provide a baseline from which continue iterating in Hybrid Spacesuit MCP-layer architectures. It is concluded that the Thesis effectively studies the potential and feasibility of the Hybrid Spacesuit concept.

Acknowledgements

I would like to take the opportunity to express my gratitude to everyone who supported me throughout the time that I needed to complete this Thesis.

First and foremost, I would like to express the deepest appreciation to my thesis advisor Allison P. Anderson. I'm thankful for their illuminating views and for continuously guiding me on the right track toward the completion of my Thesis. Without her supervision and constant help this dissertation would not have been possible.

I would like to extend my thanks to all the people working in the Bioastronautics Department at CU Boulder, specially to Katya Arquilla, Abhishektha Boppana, and Young-Young Shen. With their patience they have helped me as much as they could in any problem I had to troubleshoot. Also, I would like to extend my appreciations to Andrew S. Kerr, who as part of his undergraduate studies was part of this project and one of its main contributors. He is one of the co-authors of Chapter 2, as well as the main responsible of the Chapter 4.3 pattern sizing code.

Second, I would like to thank the Balsells Fellowship, its inspiring president Pete J. Balsells, and its coordinator at CU Boulder Robert H. Davis. Without

their support, I wouldn't have been able to develop my academic career the way that I have been able to do it at CU Boulder.

Third, I would like to give my appreciation to CU Boulder professors Francisco López and Laura Devendorf and their respective research groups, for their kind predisposition to collaborate with this project. I would like to take also into consideration the contributions to the conceptual design of the suit concept made by Michał Kracik, Ariane Chepko, and Mike Izenson. Also, this thesis wouldn't have been possible without the expert advice from Shane Jacobs.

Fourth, I want to appreciate the altruistic people from the Ocean First store. Them, along with the people working at the ITLL facilities at the University of Colorado Boulder and the CU Boulder Aerospace Machine Shop, are responsible for providing hardware and training essential to successfully develop this thesis.

Finally, I really want to thank the support received from my family, my parents and my brother, and from all my friends and beloved ones. I thank them for always being at my side giving me their love and make me always push my limits.

Table of Contents

CHAPTER 1 – The Hybrid Spacesuit as the Future of Planetary Spacesuits

I. INTRODUCTION 1

II. OBJECTIVE 3

III. PRIMARY CONTRIBUTIONS 3

IV. THESIS OUTLINE 4

CHAPTER 2 – Mathematical Approach to the Optimum Design Configuration of a Hybrid Spacesuit

I. INTRODUCTION 5

II. METHODS 6
- A. Mobility 8
- B. Feasibility 11
- C. Decompression Sickness 13
- D. System Mass 15
- E. Complexity 18
- F. Robustness 22

III. COMBINED TRADE STUDY ANALYSIS 24

IV. LIMITATIONS AND FUTURE WORK 29

V. CONCLUSION 29

CHAPTER 3 – Study on the Gas-Pressurized Layer of the Hybrid Spacesuit

I. INTRODUCTION 31

II. METHODS 33
- A. Subjects 33
- B. Hardware 35
- C. Protocol 36

III. Results 38

IV. DISCUSSION 41

V. CONCLUSIONS & FUTURE WORK 43

CHAPTER 4 – Study on the Mechanical Counterpressure Components of the Hybrid Spacesuit

I. INTRODUCTION 46

II. MATERIALS EVALUATION 47
A. Governing Principles behind MCP 47
B. Testing Method 49
C. Results 50
D. Discussion 51

III. PATTERN SIZING 52

IV. MCP GLOVE ARCHITECTURE DESIGN 57
A. Elastic Restrain Layer 58
B. Palm Pressure Distributor 66
C. Anchoring Gauntlet 70
D. MCP Layer Final Design 75
E. Design Implications 75
F. Pressure Assessment System 77

V. CONCLUSIONS 77
A. Elastic Restrain Layer 78
B. Palm Pressure Distributor 79
C. Anchoring Gauntlet 80

CHAPTER 5 – Conclusions 82

BIBLIOGRAPHY 85

APPENDIX

I. FABRICS LIBRARY 90

II. PATTERN-SIZING MATLAB CODE 93

II. PRESSURE ASSESSMENT SYSTEM 97

List of Tables

2.1 Design criteria by which system costs will be determined 8

2.2 Trade Study to determine the factors of the Complexity Equation 20

3.1 Sample means and standard deviation of the times to complete the MPPT 38

3.2 Results of the 1-way ANOVA within subjects 40

3.3 Pairwise comparisons results (p-values) using t-tests with pooled SD 41

List of Figures

1.1 Hybrid MCP-GP Spacesuit Concept 2

2.1 Pressure layer design optimization 8

2.2 Mobility equation profile 11

2.3 Feasibility equation profile 13

2.4. Decompression Sickness equation profile 15

2.5. System Mass equation profile 17

2.6. Complexity equations by suit type 21

2.7. Robustness equations specific to MCP and Gas-Pressurized suit configurations 24

2.8. Surface of the parameters' equations 25

2.9. Integrated parameters' system cost surface 28

3.1. The CU Boulder Bioastronautics Glovebox 35

3.2. The Modified Purdue Peg Test 37

3.3. Boxplot depicting the amount of time, in seconds, that each subject needed to complete each scenario 38

3.4. Boxplot depicting the amount of transformed time, in log(seconds), that each subject needed to complete each scenario 40

3.5. Some of the red skin reported by subjects 43

4.1. Definition of variables for a MCP garment cross section 47
4.2. Ideal force Displacement Curve for MCP Fabrics 49
4.3. Stress-Strain experiment on the Instron 50
4.4. Wetsuit Neoprene 51
4.5. Fabric Stress-Strain Curve 53
4.6. Fabric Thickness and Stress relation. 54
4.7. Circumference radius relation with Fabric Strain. 54
4.8. Half Circumference Function 54
4.9. Glove Pattern Design 55
4.10. Glove Pattern Ready to Print 56
4.11. Laser cut paper with the MCP pattern. 56
4.12. Elastic Restrain Layer 59
4.13. Elastic Restrain Layer v1 donned 59
4.14. Thicker Wetsuit Neoprene 60
4.15. Blind Stitch Schematic 60
4.16. Blind Stitch Used. 61
4.17. Elastic Restrain Layer v2. 62
4.18. Neoprene Cement Break-Stress test. 62
4.19. Definitive Neoprene Wetsuide Pattern cut. 63
4.20. Neoprene Cement Application. 64
4.21. Teared Neoprene Amendment 65
4.22. Elastic Restrain Layer v3. 65
4.23. Silicone Hand Mold. 67
4.24. Palmar Pressure Distributor v1. 67

4.25. PPD Putty Dough Model. 68
4.26. PPD Plaster Mold. 68
4.27. Palmar Pressure Distributor v2. 69
4.28. Palmar Pressure Distributor v3 69
4.29. Anchoring Gauntlet Preliminary Study Concept. 71
4.30. Study on the Palmar Central Restrain Anchoring. 71
4.31. Anchoring Gauntlet v1. 72
4.32. Red Skin marks due to the AGv1. 72
4.33. Anchoring Gauntlet v2. 73
4.34. 3D Printing of the Interdigital Restrain Element. 74
4.35. Anchoring Gauntlet v3. 74
4.36. Final MCP Glove design. 75

Chapter 1

The Hybrid Spacesuit as the Future of Planetary Spacesuits

I. Introduction

This Master Thesis studies a novel spacesuit architecture to enable planetary exploration of Mars in a way not feasible with currently planned mission concepts. Extravehicular activity (EVA) is a fundamental aspect of human space exploration and will be one of the main objectives for a surface visit to the Moon or Mars. Since Alexei Leonov's first EVA in 1965, the fundamental design of the spacesuit has not changed and still uses gas to create a suitable pressurized environment for the human body [1]. These suits, therefore, have the same limitations – gas pressurized (GP) spacesuits have been known to cause injuries and increase metabolic expenditure [2]–[5]. On the surface of the Moon, Apollo astronauts sustained hand, joint, and skin irritation injuries [4]. Mars surface exploration will require significantly greater ranges of motion and more frequent sorties, leading to more total time spent in EVA. This could potentially lead to higher injury incidence if the spacesuit system is not enhanced to provide long-term, healthy solutions to EVA injury [6]–[8]. With this Thesis, it is proposed a mechanism by which these limitations can be overcome by integrating a secondary, separate layer of mechanical counterpressure (MCP) to the spacesuit architecture. MCP suits provide pressure to the skin using tight elastics, mimicking the skins own functionality. Mechanical counterpressure suits offer

advantages over gas suits in that they allow for greater mobility, are lightweight, compact, and lead to lower metabolic costs due to less wasted energy [9]–[11]. Despite these advantages, these suits have not been implemented due to technical challenges to create the required level of pressure over the entire body [12], [13].

If a gas pressure garment and MCP pressure garment were combined, for example, at 2.5psi each (5psi total), the architecture has the potential to capitalize on the main advantages of each type of suit, while mitigating the primary negative aspects as well (Figure 1.1; [14]). This architecture has the potential to offer a quantifiable increase in mobility due to fewer GP components, increase in safety through pressure layer redundancy, and decreased pre-breathe time to improve operational efficiency. It could also be more lightweight, compact, and require fewer consumables. Although in concept this architecture could provide these advantages [12], [13], [15], it has not

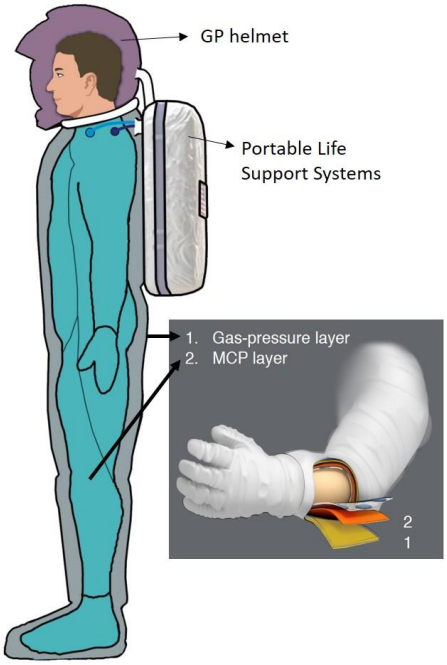

Figure 1.1. Hybrid MCP-GP Spacesuit Concept. *An inner MCP garment layer covered with a GP envelope is used to apply the adequate pressure to the astronaut. Image courtesy of Creare, LLC and Michał Kracik. [14]*

been rigorously investigated. Combining these systems could increase system complexity. Further, it remains unclear what level each pressure garment would need to be maintained at in order to create the optimal combination of these different technologies. The objective of this Master Thesis, therefore, is to explore this concept through evaluating the system architecture in all of its spectrum to determine design configurations that are the most beneficial and to provide a scientific baseline from which further work on the idea.

II. Objective

The main objective of this Masters Thesis is to perform an engineering analysis of the Hybrid Spacesuit concept. This work will serve as an initial investigation into the system architecture and serve as a baseline investigation of a hybrid spacesuit glove.

III. Primary Contributions

This Thesis aims to achieve its objective by providing 3 main contributions to Hybrid Spacesuit design:

1. Perform a trade space analysis to evaluate the most beneficial pressure contribution of the MCP and GP layers to the Hybrid Spacesuit system.
2. Investigate the relationship between gas pressure level and hand dexterity for the GP glove layer.
3. Provide design tools for MCP garment development, and develop a concept for the MCP glove layer.

IV. Thesis Outline

First, in Chapter 2, the overall Hybrid Spacesuit architecture concept will be assessed by developing a mathematical model derived from the literature. The results from this mathematical model will be used as a design-trade space to find a suitable Hybrid Spacesuit configuration regarding its layers' pressure contribution to enable planetary exploration missions.

With these results, the thesis will proceed to evaluate the gas-pressurized components of the Hybrid Spacesuit concept in Chapter 3. In this section, current proven gas-pressurized garments, not intended for EVA-rated applications, will be evaluated to determine the relationship between pressure level and manual dexterity and comfort. Testing will inform how these elements may perform when they are integrated in the Hybrid Spacesuit as one of its two pressure layers.

In Chapter 4, this thesis develops relevant tools for the development of a MCP garment intended to be integrated into the Hybrid Spacesuit. These tools provide a baseline from which continue iterating in Hybrid Spacesuit MCP-layer architectures.

Finally, in Chapter 5, the final conclusions of this Thesis are presented and discussed, and are compared with the initial objective of the thesis

Chapter 2

Mathematical Approach to the Optimum Design Configuration of a Hybrid Spacesuit

I. Introduction

In this Chapter 2, the Hybrid Spacesuit is presented, as a spacesuit architecture to enable planetary exploration of Mars by combining mechanical counterpressure (MCP) with gas-pressurization (GP). To assess the feasibility and benefit of implementing two separate pressure layers in the suit, the design space is narrowed by performing a trade analysis from the following criteria: Mobility; Technical feasibility; Risk of decompression sickness (DCS); System mass; System complexity; and Robustness. Each of these elements is then numerically modeled and system metrics are established for each to find a desirable pressure layer configuration.

So, the objective of this chapter is to explore the Hybrid Spacesuit concept through evaluating the system architecture to determine design configurations that are the most beneficial.

The work of this Chapter was published as an individual peer-reviewed paper and presented at the 48th International Conference on Environmental Systems at Albuquerque July 2018, with code ICES-2018-326. This paper was written by Roger Huerta i Lluch, Ender S. Kerr, and Allison P. Anderson and reflects their contributions as well. The entire paper will not be reproduced here but will focus on the relevant sections associated with this Master Thesis.

II. Methods

To assess the feasibility and benefit of implementing two pressure layers in the proposed Hybrid Spacesuit concept, a design optimization was performed based on relevant system architecture factors. The design space is assessed by performing a trade analysis from the following criteria, described in Table 2.1: Mobility; Technical feasibility; Risk of decompression sickness (DCS); System mass; System complexity; and Robustness.

Each of these elements is modeled numerically to represent the "system cost" (S) from each factor. The cost is a metric used to assess architectures and does not imply a monetary cost of the system (although it may ultimately be related). To normalize the contribution from each evaluation metric, the maximum value that each can take is S=1, meaning it is an extremely difficult spacesuit configuration to implement. On the other hand, S=0 is the minimum value that can be achieved, indicating the optimal spacesuit architecture, feasible and easy to implement. In the current analysis, for simplicity, each factor is given equal weighting, contributing equally to the overall system cost. Using these equations, the entire trade space will be numerically analyzed to find local minima. The targeted design regions are those with the lowest system costs values, which will be considered the most optimal spacesuit configurations.

The ratio (%) of pressure applied by MCP vs. GP will be modeled since each technology may not need to contribute an equal amount of pressure. Pressures considered will range from 0psi to 14.7psi. However, the minimum pressure

Table 2.1: Design criteria by which system costs will be determined. Total system cost will be modeled as describe for each criterion to determine design local minima. [14]

Criteria	*Description*
Mobility	Factor that describes how easy it is to perform movements. *Elevated gas pressurization will increase system cost because it decreases mobility. MCP garments will do the same, but with less loss of mobility and scale less with increased pressurization.*
Feasibility	Factor addressing the difficulty of creating a full suit. *GP configurations will have a smaller system cost than MCP because they have been widely manufactured and successfully flown. Also, elevated MCP pressurization will increase system cost because higher pressure MCP garments have not been feasible.*
DCS	Capability of the spacesuit architecture to prevent DCS. *Since it is only driven by Pressure, no difference will be appreciated between MCP and GP garments. Lower total pressure will increase system cost because it increases the risk for DCS.*
Mass	Factor addressing the total spacesuit configuration weight. *Increased mass will increase system cost in both MCP and GP garments because body-born bulk on the surface of Mars could lead to increased injury and fatigue.*
Complexity	Amount of parts needed to complete a certain configuration, which drive the capability to effectively operate over time. *Designs incorporating both MCP and Gas pressurization will increase system costs because using both technologies simultaneously will increase complexity.*
Robustness	Ability to withstand or overcome adverse conditions. *Designs incorporating only MCP or Gas pressurization will increase system costs because using both technologies decreases risk if one technology fails.*

considered in the overall system cost trade space will be 2.5psi, which is the lower possible pressure before the onset of clinical hypoxia in a pure oxygen environment [16]. A graphical representation of the design space is shown in Figure 2.1. In order to simplify the complexity of the overall trade space, only classic gas pressurized suits will be considered, while fully hard suit technologies, such as the AX-5 suit, and other emergent technologies will be omitted, and may be a topic of future research and comparison. Also, the atmosphere in the host vehicle wll be set to that used on the ISS (14.7 psi, 21% oxygen).

Each of the previously mentioned factors will be discussed in more detail. Each equation is derived based on literature or from anticipated valuation of each element.

These equations represent the preliminary system cost and establish a methodology by which to perform these kinds of spacesuit trade studies.

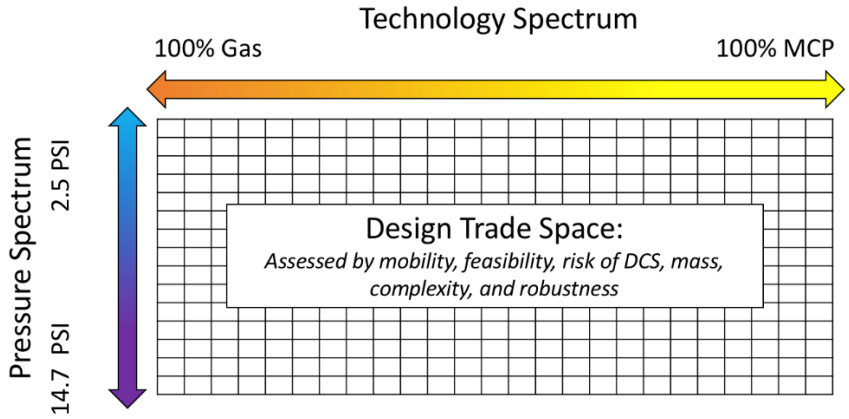

Figure 2.1. Pressure layer design optimization. *The pressure layer design will evaluate pressures from 2.5 to 14.7 PSI ranging from 100% Gas and 100% MCP pressurization technologies. The design will be optimized by the design criteria established in Table 2.1. [14]*

A. Mobility

Current GP EVA suits impose a large penalty to astronauts, as they both restrict the range of motion (ROM) and impose large resistive joint torques [17]. The mobility decrement can be caused by both a GP suit and a MCP suit. To develop equations relating the relative cost to mobility between the two technologies, a mobility comparison performed by Tanaka et al. will be used [18]. This study did a side-by-side mobility comparison of a gas-pressurized elastic glove and a GP glove. While the glove utilized in this study is not a classic fully elastic garment, it is expected to be functionally and biomechanically similar enough to enable accurate comparison of suit architectures. Utilizing a GP glove at 4.4psi, and a MCP glove that produced 9.5psi of pressure, it was observed that the range of motion for both gloves was similarly restricted. But, electromyography (EMG, a measure of muscle activation)

signals during motion was significantly less in the MCP glove than the GP glove [18]. It was also observed that EMG amplitudes did not change with pressure in the MCP garment, remaining steady at 3.3mV. While the hoop stress needed in an MCP garment does require a significant increase in material thickness with increased pressure, it does not require a commensurate increase in joint torque. Utilizing anisotropic textiles, custom fabric weaves, and/or well-designed patterns, it is possible to make the fabric resistance in one direction differ greatly from that of another, as seen in the results of this study.

Compared to the GP glove's EMG measurement of 5.2mV at 4.4psi, the MCP garment required 63.5% of the muscle activation. The change in EMG measurements will be used as an analog to joint torque. Therefore, the resistive force of an MCP glove will be 63.5% of a GP glove at 4.4psi.

A study by Mousavi et al. investigated how joint torques change with pressure in GP suits [19]. Mousavi utilized a mechanical finger stand in to apply a known torque to the finger of a GP glove at various pressures, allowing measurements of joint angle as a function of pressure to be obtained. The proximal interphalangeal (PIP) joint saw an approximately linear change in joint torque between 2.9psi and 5.8psi, leading to the conclusion that the required joint torque varies approximately linearly with increased pressure. While this is in a finger instead of full body ambulation, it is proposed as an approximate scaling analog to large joint resistance with GP suits at non-extreme joint angles. Given that the PIP joint also approximates the geometry of

other joints of interest such as the knee and elbow, it is reasonable to assume they will respond in approximately the same manner.

Linearly interpolating between the two data points given by Moussavi's research, the PIP joint torque at 4.4psi was 0.425Nm, while the same joint torque at 14.7psi would be 1.125Nm. Combining the work from these two studies, the model may be used to estimate the joint torques observed in GP gloves and the expected joint torques in an MCP glove. From this, the MCP glove was determined to require a steady 0.27Nm across all pressures.

Using these findings, a simplified model shown in Equations 2.1 and 2.2 relate the general mobility of both a GP suit and an MCP suit, with 1 set as the worst-case scenario for mobility with a GP glove at 14.7psi. A bulk knockdown factor of -0.05Nm is also implemented in the MCP equation to acknowledge the materials properties of the suit, where an MCP suit is a skintight garment, compared to the bulky bladder required by the GP suit. Figure 2.2 shows these equations for each suit type plotted by pressure and system cost S.

$$S_{gas} = \frac{\frac{1}{14.7}P_{gas} + 0.125}{1.125} \tag{2.1}$$

$$S_{MCP} = \frac{0.27 - 0.05}{1.125} \tag{2.2}$$

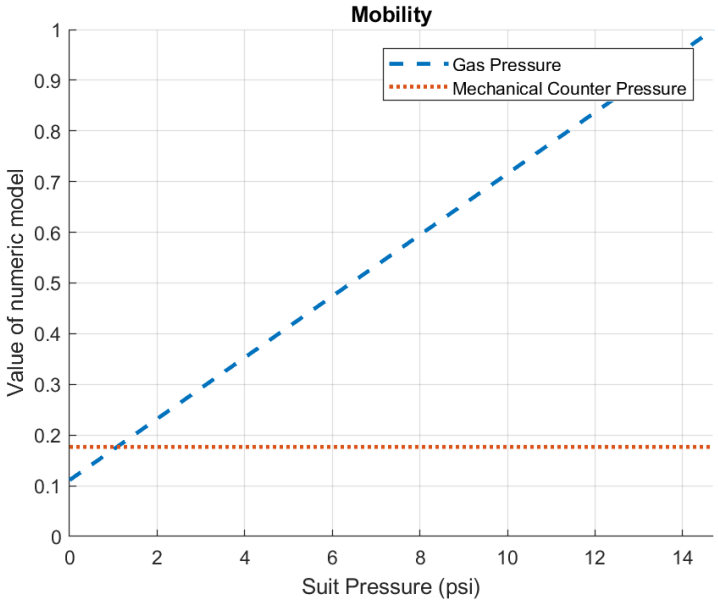

Figure 2.2. Mobility equation profile.

B. Feasibility

For our purposes, feasibility will be defined as the difficulty of creating a full suit at a given pressure, using only current technology and maintaining reasonable mobility and weight. It is not a measure of the system's ability to conform to mission requirements, but rather a measure of the difficulty in developing hardware that generates the requisite pressure.

The MCP equation will be defined by the previous full body suit that was developed by Webb, and the current estimated maximum achievable pressure generation using MCP over the whole body. Webb successfully created a mechanical counter pressure of 3.5psi over the entire body [9]. Given that Webb's suit was a technology demonstrator, and that a flight suit would be more difficult to develop, the feasibility of a 3.5psi MCP suit is set at twice that of a typical launch and entry suit. The MCP curve will be linear from zero to one, through this reference point. Above the intersect

point of 8.6psi, where feasibility reaches a value of 1, the MCP suit above those values will remain a 1.

GP suit architecture is more thoroughly investigated given the history of achieved spacesuit configurations. In the U.S., suit pressures below 4.3psi are within our known design ranges, with many suits, particularly launch and entry suits, operating at 3.5psi. Zero-prebreathe suits, such as the Mark III, were designed to operate at 8.3psi [20]. Given the demonstrated feasibility, but the relative lack of design points between 4.3 and 8.3psi, a value of 0.25 is assigned to suits within these ranges. Suit pressures below 4.3psi will linearly fall to 0, and anything above 8.3psi will linearly rise to 1. Figure 2.3 shows the graphical representation of these curves, presented in Equations 3 and 4.

$$S_{gas} = 0.0581P_{gas}\ ;\{0 \le P_{gas} < 4.3\}$$
$$S_{gas} = 0.25\ ;\{4.3 \le P_{gas} < 8.3\}$$
$$S_{gas} = 0.1172P_{gas} - 0.7226;\{8.3 \le P_{gas}\} \quad (2.3)$$

$$S_{MCP} = 0.1162P_{MCP}\ ;\{0 \le P_{MCP} < 8.6\}$$
$$S_{MCP} = 1\ ;\{4.3 \le P_{MCP}\} \quad (2.4)$$

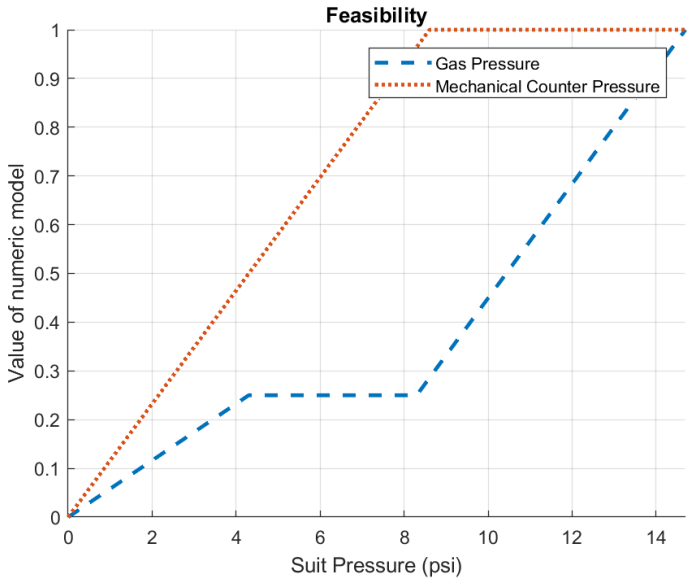

Figure 2.3. Feasibility equation profile.

C. Decompression Sickness

Decompression Sickness (DCS) is caused by rapid changes in environmental pressure. This factor is only driven by pressure and not by which system applies that pressure, so no difference will be appreciated between MCP and GP garments equations. Prior to DCS, a measure of tissue stress is the appearance of Venous Gas Emboli (VGE) in the blood. These measures are correlated but not equivalent [21]–[23]. This medical issue is mainly driven by tissue saturation with nitrogen (N_2) and the time at the reduced pressure. Haldane's Ratio (R) sets the risk of DCS. This value computes the ratio of N_2 stress in the body (Eq. 2.5), being the partial pressure of nitrogen (ppN_2) after the prebreathe protocol, and P_f the final pressure. As DCS is probabilistic, it is considered that the body can handle some stress. Each space agency has different R thresholds, depending on the amount of risk they are willing to accept [24]. On the ISS R is set to 1.4 and is used for our equations (although in contingency

purge flow operations up to R=1.80 is allowed for no longer than 30 minutes). At this R level, bubbles may be present in the blood, or even 35% of cases with bubbles at the heart. Up to 5% of subjects experience DCS symptoms, too.

$$R = \frac{ppN2}{Pf} \tag{2.5}$$

One assumption for this model is that spacecraft atmosphere will be maintained as on the ISS, with a pressure of 14.7psi. Data from the NASA Mans System Integration Standards indicates prebreathe times to achieve R = 1.4. The equation is normalized, where longer prebreathe times are the worst-case scenario (i.e. at time=435min, P=2.5psi, S=1). The 2.5psi pressure level is considered the worst-case scenario (S=1) because below this pressure a human starts being affected by clinical hypoxia (oxygen pressure in the alveolus under 1.16psi) [16]. On the other extreme, any pressure equal or over 8.3psi doesn't require a pure oxygen prebreathing time when coming from a 14.7psi environment [25], so any pressure over 8.3psi will be considered the optimal scenario (S=0). Figure 2.4 shows the values represented in Equation 2.6.

$$\begin{aligned} S_{DCS} &= 0\,;\{8.3 \leq P \leq 14.7\} \\ S_{DCS} &= \frac{625 - 76P}{435}\,;\{2.5 \leq P < 8.3\} \\ S_{DCS} &= 1\,;\{2.5 > P\} \end{aligned} \tag{2.6}$$

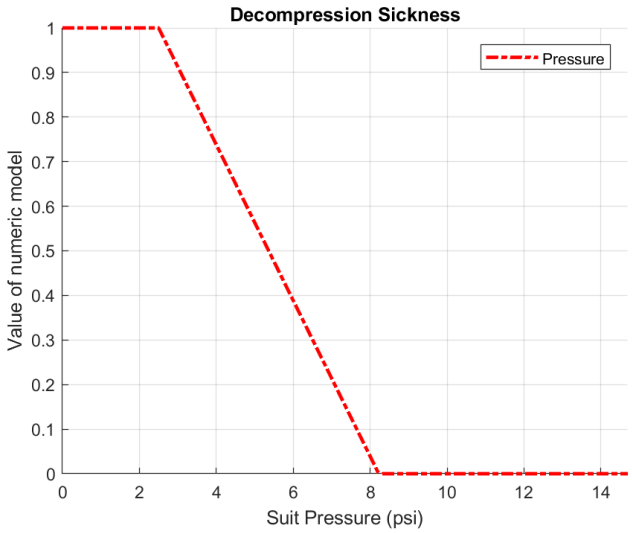

Figure 2.4. Decompression Sickness equation profile.

D. System Mass

Comparing the mass across MCP and GP suits and the relationship between suit pressure and system mass is challenging with few design cases to reference. To anchor mass estimates to real world data, a comparison between historical suit architectures from the same development era will be used. While the mass of the system, particularly the consumables, may change with differing EVA profiles, this may be compensated for via the end weighting of the system instead of initial changes to the model if required.

The Apollo era AL7 spacesuit had a mass of 201lbs [26], 125lbs of which was comprised of the Personal Life Support System (PLSS) [1]. Webb states that a MCP suit would require approximately half of the life support mass for a planetary exploration, with half of the mass coming from the thermal control system (TCS), and half coming from the PLSS [9]. For non-planetary exploration, full active thermal control must be maintained. These factors place the mass of an MCP suit's PLSS and TCS systems at 75% of the Apollo era spacesuit mass. Webb further states that the

MCP suit itself may be safely expected to be 25% the mass of a GP suit. Therefore, it may be concluded that the full system mass of a MCP suit at Apollo suit pressures (3.7psi) will be half that of the Apollo baseline, at 100.5lbs.

To assess how the mass of an MCP system varies with pressure, suit materials properties are determined. MCP relies upon the hoop stress in the circular cross sections of fabric to generate pressure through tension, which may be approximated for thin wall sections via the hoop stress equation (Eq. 2.7).

$$\sigma = \frac{PD}{2t} \tag{2.7}$$

Where P is the pressure, D is the Diameter of the section, and t is the thickness of the material. If the stress is held at a constant value, then the material thickness must scale linearly with pressure increase at a set diameter. Using the approximate density of a nylon type plastic, at 1400kg/m^3, and the average surface area of a large male human, at 1.9m^2, and an initial average suit thickness of 1mm at 3.7psi, the mass of an MCP suit will increase with a slope of 23.44lb/atm. This extrapolates to a nearly 0psi suit mass at 94.6lb.

The mass of a GP suit is assumed to vary linearly with pressure if the mobility factor is held constant. This necessitates the addition of multiple hard bearings and other mobility enhancing additions, leading to a large increase in mass as pressure increases, due to the constant mobility constrain that we have imposed when considering this aspect of the system. To anchor the GP suit, first the stated mass of 201lbs at 3.7psi is used.

It is then assumed that the weight of a nearly 0psi GP suit will be equal to that of a nearly 0psi MCP suit. At a base level, either suit that produces zero psi is merely a full body covering, analogous to two similar flight suits. Therefore, the slope of the mass of the GP system is 422.7lb/atm, placing a 14.7psi GP suit with the same mobility as the Apollo suit at 517lbs. The previously stated values provide the anchor points for both suit types and Equations 2.8 and 2.9 are the linear fits to these points. Equations 2.8 and 2.9 are shown in Figure 2.5. While it is possible to fully normalize the equations, it is felt that there should always be some penalty associated with the inherent weight of the system.

$$S_{gas} = \frac{94.6 + 422.7\frac{P_{gas}}{14.7}}{517} \tag{2.8}$$

$$S_{MCP} = \frac{94.6 + 23.44\frac{P_{MCP}}{14.7}}{517} \tag{2.9}$$

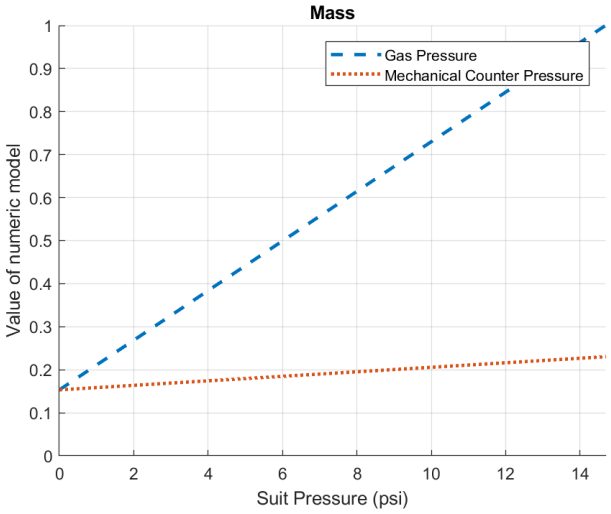

Figure 2.5. System Mass equation profile.

E. Complexity

Complexity is usually expressed as the number of parts needed to complete a system and drives the capability of a system to effectively operate over time. The more complex a system is, the more it is susceptible to degradation, malfunction, or disassembly of its internal pieces. As the pressure applied to a person increases, the amount of different systems to do so also increases. For example, when using a GP system, pressure drives the need for gas storage, delivery of the gases inside the suit, more consumable weight, and strength of the pump, which consumes electricity and space. When using a MCP pressure layer, additional elements such as gas tightening bladders have historically been used to achieve the desired pressure [27]. Importantly, designs incorporating both MCP and GP will have additional complexity and increase system costs to integrate the different technologies.

Separate Complexity equations are developed for each pressure mechanism to reflect their differences. The parameters considered to assess complexity are the pressure layer complexity, the number of elements that they need, the don/doff times, and the ability to maintain uniform pressure all over the body. Each of these parameters is weighted for their relative contribution to overall system complexity. The weights are scored using values between 1-4, being 1 “not important” and 4 “extremely important”. This is then multiplied by the range within the parameter the technology lies on a scale from 1-10, with 1 being “really simple” and 10 “extremely complex”. For some, there is not a single scale, but rather is dependent on the

pressure extremes being considered. Table 2.2 shows these numerical weightings, but are described as follows:

- **Pressure layer complexity** (2): The MCP pressure layer can range from a very simple low-pressure passive elastic garment, to a very complex system design in order to achieve high pressures. It is therefore given the range from 3 to 9. The pressure garment for the GP suits have an inherently higher complexity, due to the patterning and required bladder and restraint layers [10], [13], [15]. These elements are required to a greater degree at higher pressures. Therefore, it is assigned the range from 5 to 10.
- **Number of elements** (4): As stated before, the number of elements of each of the systems is dependent on the pressure needed, as well as the mobility desired to achieve [10], [12]. For higher pressures, more elements will be needed to maintain the same mobility capabilities. Baseline configurations of MCP suits required fewer components than GP suits and are therefore given the range from 1-4 while the GP system has a range from 7-10.
- **Don/doff times** (1): Don/doff times for MCP suits are highly dependent on the pressure of the garment. They are therefore assigned the full range from 1 to 10. Alternatively, gas suit don/doff times are not dependent on the pressure, but rather the implemented configuration (i.e. rear entry hatch vs. modular system). Historically, Webb's MCP suit needs a team of 3 people to don it in 30 minutes (3x30=90 work-minutes) [9] while the GP suit requires two people, one being the person wearing the garment, to don in 15 minutes (2x15=30 work-

minutes) [28]. Therefore, for a moderate pressure, the GP is easier to don, so the value is set to a constant of 3.

- **Uniform pressure capabilities** (3): The GP allows a nearly-perfect distribution of pressure all over the body with ease. It is therefore assigned a value of 2. MCP garments are much more susceptible to the pressure required. Particularly over non-uniformities of the body, such as the concavity of the palm of the hand, it is challenging. It, therefore, ranges between 5 and 10 [29].

Table 2.2: Trade Study to determine the factors of the Complexity Equation

		MCP				GP			
		Normalization Factor		Total		Normalization Factor		Total	
	Wt factor	Best Scen.	Worst Scen.	Best Scen.	Worst Scen.	Best Scen.	Worst Scen.	Best Scen.	Worst Scen.
Pressure Layer	2	3	9	6	18	5	10	10	20
# Elements	4	1	4	4	16	7	10	28	40
Don/Doff Time	1	1	10	1	10	3	3	3	3
Uniform Pressure	3	5	10	15	30	2	2	6	6
		MCP Total Values:		**26**	**74**	**GP Total Values:**		**47**	**69**

The weights of the parameters are used with the range described to find the best and worst-case scenario for both technologies. The lowest score is MCP at low pressures. This intercept is removed from both equations, so the line for MCP, which has the lowest overall best-case scenario, has a complexity of 0. Therefore, the GP has a higher initial offset in complexity. The slope each line is set by the difference between the best and worst-case scenarios. The entire equation is then normalized by the highest worst-case scenario, also from MCP, to convert the complexity scale to be between 0 and 1. Equations 2.10 and 2.11 represent these equations and are shown in Figure 2.6A.

$$0psi < P_{mcp} \leq 14.7psi\ ;\ S_{mcp} = \left(\frac{(74-26)}{14.7} P_{mcp}\right)/74 \tag{2.10}$$

$$0psi < P_{gas} \leq 14.7psi\ ;\ S_{gas} = \left(47 - 26 + \frac{(69-47)}{14.7} P_{gas}\right)/74 \qquad (2.11)$$

In addition to the complexity inherent in each technology, an additional factor of complexity should be included when the systems are combined. There should be a noticeable increase of the complexity when both systems are present. It is achieved with an additive sine function governed by Equation 2.12. It is scaled such that when 50% of the pressure is produced by each technology at the highest pressure configuration, the system complexity is approximately 33% of the total complexity (i.e. 33% of the complexity comes from the GP, 33% from the MCP, and 33% from the combination of technologies). The value in this configuration is a sine wave with an amplitude of 0.25 (Figure 2.6B).

$$S_{union} = 0.25 \sin\left(\frac{\pi}{2} * \frac{\%(100-\%)}{2500}\right) \qquad (2.12)$$

The Complexity Equation is created as the sum of each of the 3 system costs, calculated from Eq. 2.10, 2.11, and 2.12, shown in Eq. 2.13.

$$S_{complexity} = \frac{S_{mcp}+S_{gas}+S_{union}}{S_{max}} \qquad (2.13)$$

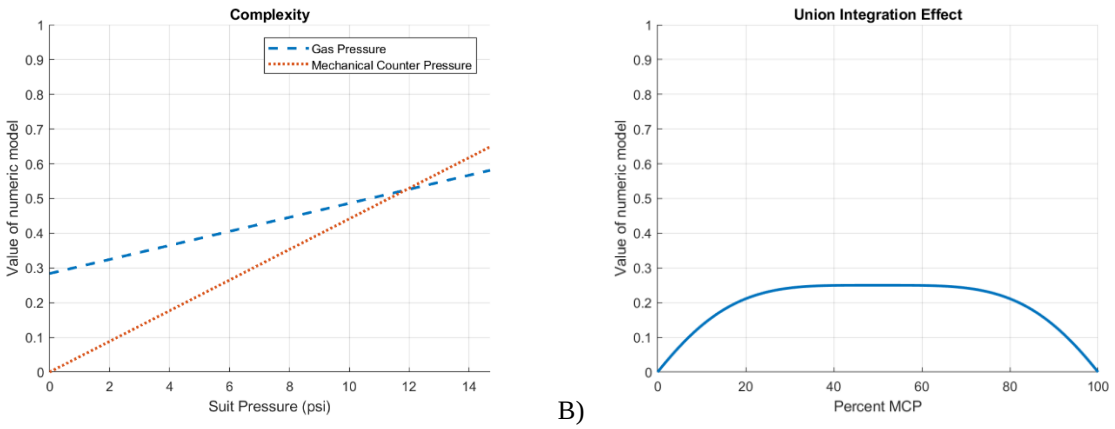

A) B)

Figure 2.6. Complexity equations by suit type. *The two suit styles have different complexity slopes (Figure A). The union of two suits at nearly equivalent pressure will likely increase system complexity (Figure B)*

F. Robustness

Robustness is defined as the ability to withstand or overcome adverse conditions, designs incorporating only MCP or GP will increase system cost because using both technologies together decreases risk if one technology fails. Failure mechanisms result in loss of pressurization of a given layer. Costs will incorporate the pressure of each technology independently by pressure, then the system costs will be summed.

MCP is less dependent on redundancy systems, yet it can still be affected by exogenous problems like MMOD impacts, so its lowest safety factor is set to S_{robust}=0.1. If the garment is punctured, a pressure gradient is localized around the hole location and the rest of the body. While this effect would be local, if this scenario happens with a GP garment, the effect would be on the pressure applied to the entire body, when the "feed the leak" capabilities with redundant oxygen have been exhausted. Also, MCP garments can be repaired while worn. For example, putting a strap over the hole, applying a tourniquet style compression, would be enough to counteract the tear [29]–[31]. Additional cost considerations for GP suits are their sensitivity to punctures and impacts, leakiness, and is susceptibility to dirt and dust [10]. Therefore, the minimum safety factor will be S_{robust}=0.3.

There is no advantage in robustness to maintaining pressures equal or higher than 8.3psi when both technologies are used together. Once 8.3psi pressure is achieved in the redundant pressure layer, any increases in pressure don't provide additional protection against DCS. From this pressure to the most extreme hypoxic environment where humans can still breathe and assimilate oxygen (2.5psi) the safety that each

of the systems provides decreases as the pressure decreases. This is due to the fact that they still provide enough pressure to the astronauts, so they can still be operative, but these levels less optimal. So, the safety factor in this interval increases up to 0.1 for both systems.

Below the threshold of 2.5psi, the robustness of the system quickly decreases, with the greatest costs when the redundant technology is not present in the system (P=0psi, S_{robust}=0.5). Although between 0 and 2.5psi pressure levels can't effectively protect the astronaut, the redundant pressure layer does add some buffer, increasing robustness. Equations 2.14 and 2.15 represent the Robustness cost, and is shown in Figure 2.7:

$$P_{gas} \geq 8.3psi\ ; S_{gas} = 0.3$$

$$2.5psi < P_{gas} < 3.5psi\ ;\ S_{gas} = 0.3 + \frac{1}{58}\left(8.3 - P_{gas}\right)$$

$$P_{gas} \leq 2.5psi\ ;\ S_{gas} = 0.4 + \frac{1}{25}\left(2.5 - P_{gas}\right) \tag{2.14}$$

$$P_{mcp} \geq 8.3psi\ ;\ S_{mcp} = 0.1$$

$$2.5psi < P_{mcp} < 8.3psi\ ;\ S_{mcp} = 0.1 + \frac{1}{58}\left(8.3 - P_{mcp}\right)$$

$$P_{mcp} \leq 2.5psi\ ;\ S_{mcp} = 0.2 + \frac{3}{25}\left(2.5 - P_{mcp}\right) \tag{2.15}$$

The Robustness equation will be the summation of both terms (Eq. 2.16).

$$S_{robustness} = S_{mcp} + S_{gas} \tag{2.16}$$

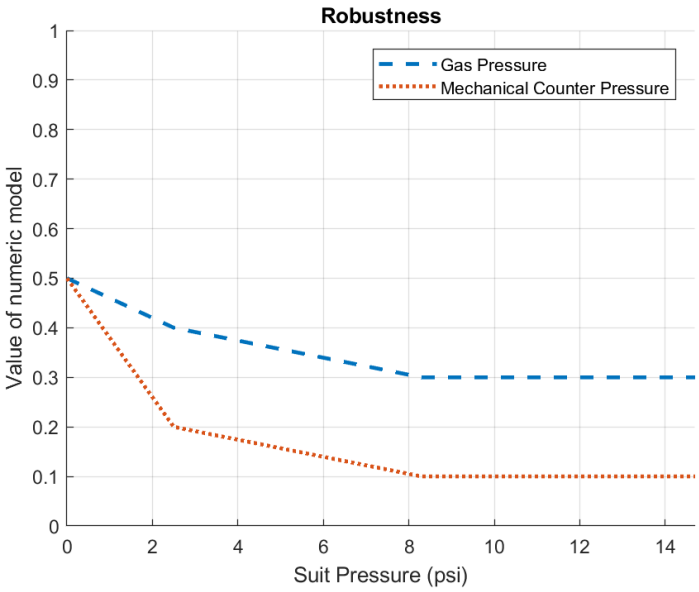

Figure 2.7. Robustness equations specific to MCP and Gas-Pressurized suit configurations. *The total score of the equation is the sum of the two elements*

III. Combined Trade Study Analysis

The combined analysis was performed by plotting and merging all the factor's equations using MATLAB [32]. The inputs of our equations were the total pressure of the spacesuit (P) and the proportion of pressure amount being applied by the MCP garment (MCP%). The pressure values that were considered ranged from 2.5psi, the lower possible pressure before the onset of human clinical hypoxia in a pure oxygen environment [16], to 14.7psi, Earth's surface atmospheric pressure. The MCP% ranges between 0 and 100%, intrinsically establishing that the proportion of GP system in each point is its opposite (GP% = 100 – MCP%). The populated data derived from each one of the factors' equations is plotted as surfaces, shown in Figure 2.8. For all the equations, as well as for the overall system cost equation, 0 is considered as the best scenario (lowest system cost configuration) and 1 is considered to be the worst scenario (highest system cost architecture). The best scenarios (S values near to 0)

were given cold-blueish colors, while worst case scenarios (S near 1) were given hot-reddish colors. After plotting all the different parameters, it can be seen how each contributes independently to the overall system cost design trade space.

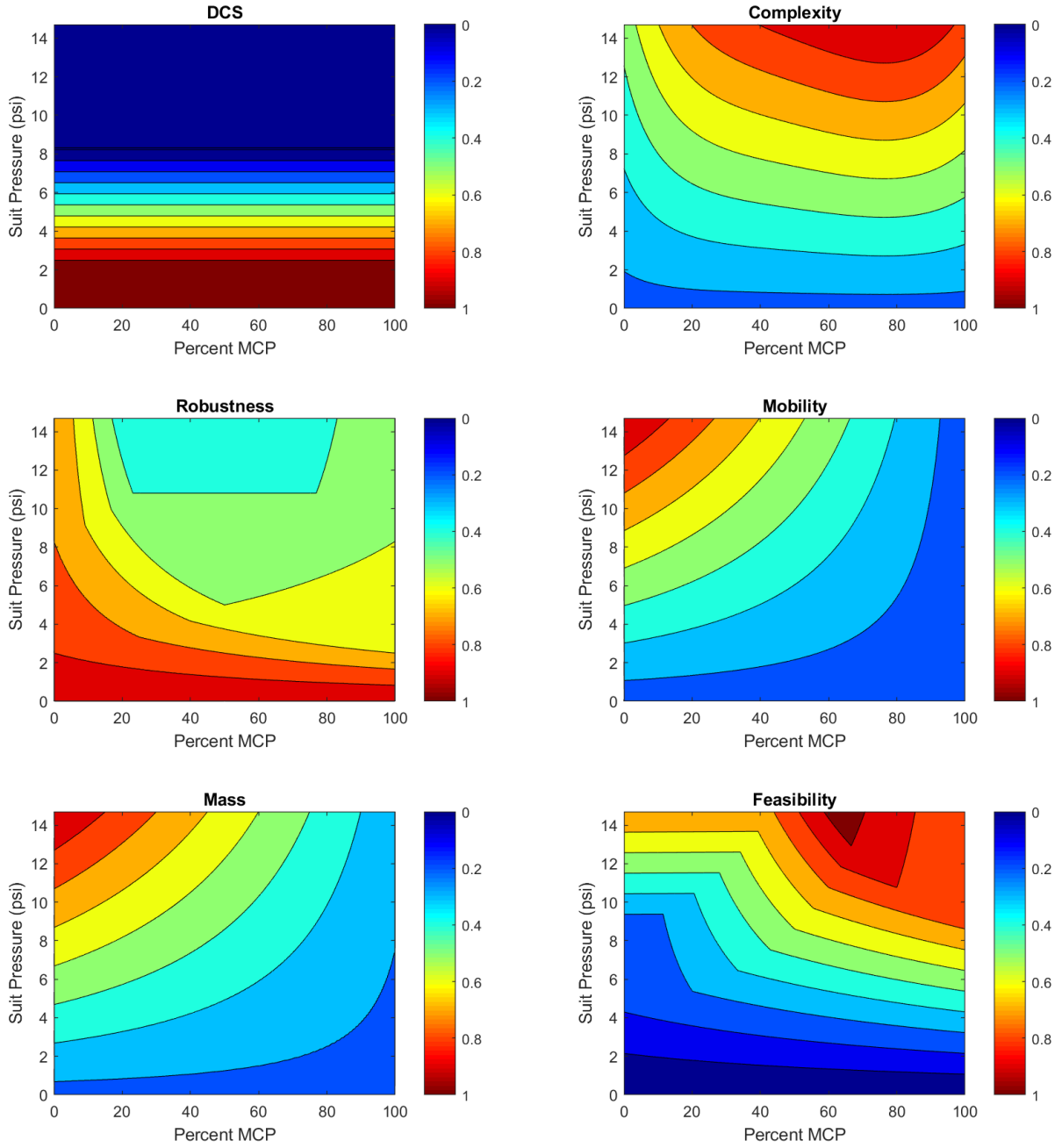

Figure 2.8. Surface of the parameters equations. *The areas with lower system costs (optimal configurations) are those with values near to S=0 and painted with cold/blue colors; the areas with higher system costs are those with values near to S=1 and are displayed with hot/red colors.*

From a pressure perspective, it can be seen in Figure 2.8 that DCS and Robustness parameters are the ones that benefit high-pressure scenarios. These two parameters take into account the importance of maintaining a good physiological health when wearing the spacesuit. As the pressure at which the human body is most used to is the Earth's pressure at sea level (14.7psi), the pressures nearer to this value are the ones considered to be healthier and safer. Subsequently, high pressures are the ones with lower system costs. On the other hand, the lowest system costs of Complexity, Mobility, Mass, and Feasibility factors can be found in the lowest pressures of the trade space. These factors are mainly driven by the characteristics of the mechanical components used in each spacesuit configuration. Mechanical components usually perform better when they are not under heavy stress and have less interaction between them, resulting in less fatigue and longer mean times before failure. So, as lower pressures mean fewer components and less workload applied to them, all of these parameters have their optimal and lower system costs in low-pressure regions.

From a MCP usage point of view, the factors being plotted in Figure 9 that have lower system costs in high levels of MCP usage are Mobility and Mass parameters. This correlates with current literature, which establishes these two parameters as two of the main benefits of MCP garments [12], [13]. Their capacity to reduce bulk is translated into lighter and more dexterous spacesuit configurations. On the other hand, Feasibility graphic shows that it benefits low MCP levels over configurations with higher MCP participation. This is consistent with our historical context that all spacesuits flown to the date are 100% GP, so these are more feasible and easier to be

implemented. Finally, the other parameters (DCS, Complexity and Robustness), as are mainly driven by pressure, they don't show to be strongly influenced by the MCP levels.

To assess the integrated system cost equation, what is performed is the summation of the system costs (S) for each factor. Then, the value is normalized by the weighting factors to set the overall system cost valuation also on a scale from 0 to 1. The integrated overall system cost equation is shown in Equation 2.17. In this analysis, each factor was given equal weighting ($A = B = C = D = E = F$).

$$f(P, \%MCP) = \frac{Af_{mobility} + Bf_{feasibility} + Cf_{DCS} + Df_{mass} + Ef_{complexity} + Ff_{robustness}}{A+B+C+D+E+F} = S \qquad (2.17)$$

By combining each factor into the overall architecture cost simulation, the integrated surface, shown in Figure 2.9, indicates that when all parameters are equally weighted, there can be found two main optimal zones painted in yellow (those with lower system cost values) for a Hybrid Spacesuit configuration combining MCP and GP garments.

The first region of interest is the area that can be found around P=8.3psi, pressure achieved with approximately 30-40% of MCP and 60-70% or more of GP. The second is a larger area to the right of the graph, with high MCP levels (>60%) and pressures ranging from 5 to 11psi. The first area shows a design configuration where optimal designs are achieved with a combined low level of MCP with a GP spacesuit. The second area shows the capabilities that MCP suits could have if they were the dominant source of high pressures.

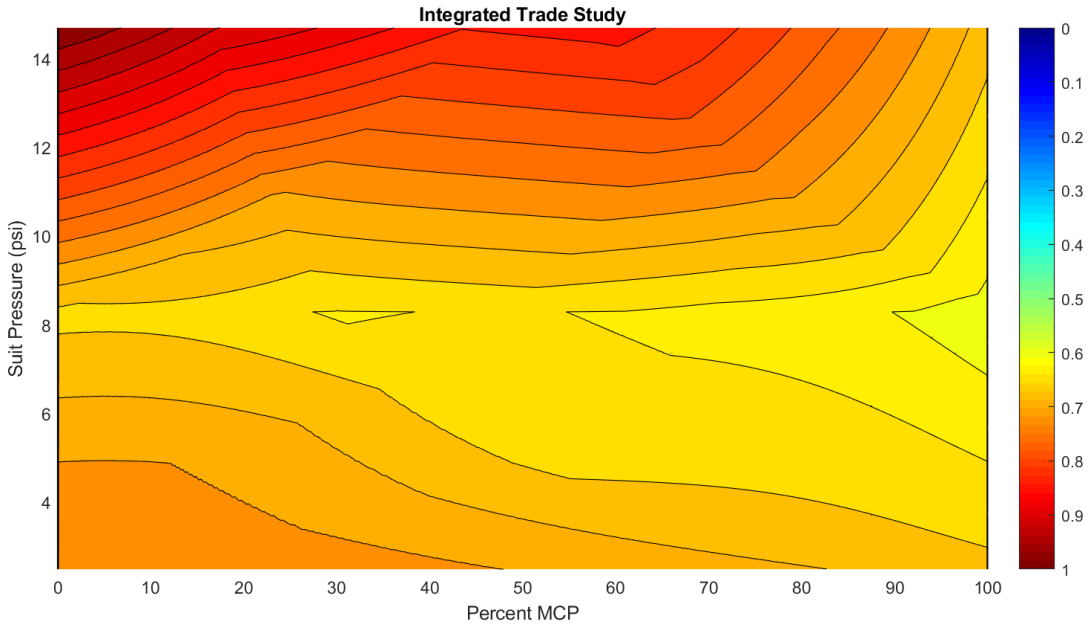

Figure 2.9. Integrated parameters' system cost surface. *The areas with lower system cost (optimal configurations) are those with values near to S=0 and painted with cold/blue colors; the areas with higher system costs are those with values near to S=1 and are displayed with hot/red colors.*

Since this second area, though, is unlikely to be technically feasible given the current state of MCP technology, the first region is of greater interest to explore. Within this space, there are several designs that could be achieved. For example, a configuration within this space would provide 2.5psi with a MCP garment and the remaining 5.8psi with a GP one. A 5.8psi suit is well within the design regimes for GP suits, since this is the operating pressure of the Russian Orlan spacesuit. This analysis, though, is only one potential evaluation, particularly since all factors were weighted equally. For future architecture design, the importance of each factor independently should be assessed against mission objectives, and used to tune the model to achieve an assessment of desirable configurations.

IV. Limitations and Future Work

The results presented are founded on the spacesuit literature from historical spacesuit designs and estimations of trades between the two concepts. This work can be further refined to incorporate additional information to anchor the equations. The pressures are varied between but not including 0% MCP (which is 100% GP) and 100% MCP, (which is 0% GP). Future work includes comparing the hybrid designs to solely GP or solely MCP, which were excluded in this trade study. As programmatic objectives, and as suit designers perform their trade studies, each factor can be weighted differently to increase or diminish its relative importance. Future work performs these trades by changing the weighting of each factor to determine the sensitivity of the trade study on a given factor.

From the results of the pressure layer determination, a more detailed conceptual design will be conducted. In particular, this effort will focus on the capabilities and characteristics that both pressure layers should have in order to be integrated in the Hybrid Spacesuit. Additional future work investigates how currently available materials can be used as the construction materials of these layer, and how they may be affected by this pressure garment concept.

V. Conclusion

There is a long legacy of spacesuit hardware that successfully used gas-pressurized spacesuits to safely perform EVAs. As we move to surface exploration where there will be sustained EVA effort, the limitations of gas-pressurized suits become more apparent since they inhibit mobility, cause fatigue, and lead to injury. MCP suits, on

the other hand, have not demonstrated the technical feasibility required to sustain the human body in vacuum for long durations yet. The exception to this was the full body suit produced by Webb [9], but this suit suffered from operational constraints making it infeasible. To shift the paradigm of thinking of these technologies as independent, it is proposed a Hybrid Spacesuit concept and investigate its potential advantages and feasibility. A trade study was performed on system architectures to fuse these technologies, considering the risk of Decompression Sickness, Robustness, Complexity, Mobility, Mass, and Feasibility. After performing this factorial analysis, a promising spacesuit configuration is detected: the zone with the smallest system cost is found around a spacesuit pressure of 8.3psi, 40% or less of this pressure being applied by a MCP garment. However, this result is susceptible to future re-weighting of each factor contribution to the overall trade study.

The objective of this chapter is to establish a spacesuit trade study methodology that can provide an unbiased evaluation of the spacesuit design. Further, it is adaptable as new technologies either increase the effectiveness of GP suits or increase the feasibility of full body MCP suits. With this work, it is hoped to further the feasibility of such a suit concept for future implementation in planetary exploration suits, as well as providing a baseline scenario that sets the objectives from which start iterating on the development of the concept.

Chapter 3

Study on the Gas-Pressurized Layer of the Hybrid Spacesuit

I. Introduction

The results from Chapter 2 inform the pressure at which the GP layer of the Hybrid Spacesuit concept should be maintained for a specific planetary surface exploration scenario. Following the conclusions of that same chapter, the different parameters had to be further evaluated to better identify their relations with the overall system costs. Chapter 3 focuses exclusively on investigating more thoroughly the relation between Mobility with gas-pressure.

In a study conducted by Mousavi et al.[19], the relationship between pressure in a gas-pressurized spaceglove and the dexterity of its user ("Mobility" parameter in the study from Chapter 2) followed a linear progression (Figure 2.2). However, there were three limitations with that study: 1. not all the finger joints showed a linear relationship between pressure level and dexterity; 2. single joint movements were studied, not the integrated motion of the hand, which is more important for operational settings.; 3. they used an Orlan-DM glove, which is a more complex glove and does not enable efficiencies in design that lower pressure gloves may want to take advantage of.

Data for the mathematical model is based on current EVA-rated gas-pressurized spacesuits components. However, such complex and unique accommodations for these

components may not be required in certain Hybrid Spacesuits. For example, if a 4psi Hybrid Spacesuit configuration is considered with a 50% MCP participation, just 2psi should have to be sustained by the GP layer. This pressure can be achieved with commercially available components, such as pressurized high-altitude suits used by pilots and paratroopers over decades. These are much cheaper and easier to manufacture than spacesuits [33]. Using a suit like this as one of the layers of the Hybrid Spacesuit would also reduce system complexity, thus it may be more feasible to produce and operate than current EVA quality gas-pressurized spacesuit.

The main objective of this chapter is to overcome these limitations identified in the previous chapter when assessing the mobility parameter (dexterity from now on) and gain more insight into the relationship between the mobility and a gas pressurized garment, using a pressurized glove. The secondary motivation of Chapter 3 is to investigate simplified gas-pressurized glove hardware by assessing its dexterity with changes in pressure level.

To achieve these objectives, a study was designed that compares the gas pressure levels of a pressurized glove against the dexterity capabilities of its users. The hypothesis that this study aims to test are:

1. The dexterity tasks are performed significantly different using a pressurized glove at 2psi than at 3.5psi.
2. The dexterity tasks are performed significantly different using a pressurized glove at 0psi than at 2psi.

Also, to ensure the dexterity decrements are due to the glove and not the experimental test set up, three different baseline scenarios are investigated. This baseline scenario will be compared against those in which the pressurized glove is donned and pressurized. Secondary hypotheses are:

3. The dexterity tasks are performed significantly differently when performing it inside the glovebox than outside it.
4. The dexterity tasks are performed significantly differently when performing it inside the glovebox with the unpressurized glove donned than when they are performed barehand inside the glovebox.

Performance will be evaluated by calculating task completion time. The time to perform certain activities, such as the Purdue Peg Board procedure or knot tying [17], [34], can be used to evaluate the dexterity capabilities of a glove. So, following those, the time that each subject needs to complete a certain task will be the variable used to compute the statistics analysis: the quicker the tasks are performed, the better the dexterity of the user will be considered. The precise development and results analysis of the study are shown in the following sections.

II. Methods

A. Subjects

The data that was collected is conformed by non-probability samples, as it was a convenience sampling. All participants were Engineering students at CU Boulder, ranging from 21 to 23 years old. The participation of these subjects in the study didn't

require IRB approval, as the data was collected during a graduate class and IRB stated it so.

A power analysis was conducted [35] using the information provided in the study performed by Bishu & Klute in 1995 [17]. With a power of $(1-\beta) = 0.97$, it was considered that 2 people were the minimum number of samples per scenario needed to be able to drive significant results.

Additionally, if at least 6 subjects were tested per scenario, it would be easier to compare the results with other studies such as the study conducted by Bishu & Klute in 1995 (6 subjects, 3 males and 3 females).

A total of 7 male subjects were tested. Of these, 5 were right-handed and 2 were left-handed. No subject had any previous relevant experience with spacesuit gloves. Initially, 4 female subjects were as well recruited and tested, but were excluded from the study due to 3 being unable to complete all the MPPT scenarios. The reason behind that is thought to be hand-size as some subjects were found to have their hand sizes fall under the 15^{th} percentile of the female population [36], meaning that their hands were too small for the glove that was used. So, with just one female subject, it was decided all female samples to be discarded from further analysis.

Also, considering the left-handed subjects, any exploration of possible covariance of this parameter was not performed. This parameter was integrated in the error intrinsic to each subject between the other ones. Additionally, although subjects maybe had relevant different hand sizes, they were not measured as it was considered

that if they were able to complete all MPPT scenarios they were suited enough to be considered in the study.

B. Hardware

A pressurized left-hand glove for high-altitude environments was used. Although just having a single size, the glove could be adjusted with a restraint line on the palm.

The glove was pressurized using a custom built glovebox in the Bioastronautics Laboratory at CU Boulder (Figure 3.1). By creating a vacuum in the glovebox, the pressure differential with ambient atmospheric pressure creates a "pressurized" glove. This glovebox has the ability to have its internal pressure to be dropped up to -8.3psi. However, as the maximum operable pressure of the glove was -3.5psi this pressure differential was never exceeded during the study. The extremely low leaking rate of the glovebox maintained constant glove pressure for more time than the needed for the testing.

Figure 3.1. The CU Boulder Bioastronautics Glovebox. *used in this study and capable of lowering its internal pressure down to -8.3 psi without appreciable leaking.*

C. Protocol

The independent variable of this study was the Glove Condition. There were 5 different conditions:

1. Barehand, Outside the Glovebox
2. Barehand, Inside the Glovebox
3. Glove, Inside the Glovebox, 0psi
4. Glove, Inside the Glovebox, 2psi
5. Glove, Inside the Glovebox, 3.5psi

This would be a repeated measures within-subject effect fixed design. Our dependent variable was the Time Required to solve the dexterity task, measured in seconds.

From literature [17], different possible confounds, source of variability between subjects, were detected: dominant hand, sex, previous experience, and hand size. Also, it was decided that any upper extremity impairment was considered enough for exclusion criteria.

A modified Purdue Pegboard test (MPPT) was used in this study since it had been used previously by NASA to evaluate glove performance [34]:. As it can be seen in Figure 3.2, the MPPT consisted of picking up 10 U-bolts from the Pegboard in order, turning them 90 degrees, and placing them again in the Pegboard. The order of which U-bolts they picked first was standardized and equal for all subjects. This MPPT procedure allowed a good interaction between the gloves and the pegboard (as the bolts are bigger (5/16”), as it is considered that traditional medical pegs used in the

Purdue Peg Test were too small to be manipulated with pressurized gloves. The MPPT also forces the user to not just use the fingers but also the wrist (to properly do the 90 degrees turn).

In order not to have any learning curve or tiredness effect during the test, each subject had a different test scenario order, completely randomized.

Also, subjects were required to practice the MPPT without the glove and outside the glovebox at least three complete times before beginning the experiment, but they could repeat the procedure additional times as they needed to get familiar with the task. Only one time was recorded per scenario.

Figure 3.2. The Modified Purdue Peg Test *used to evaluate dexterity based on time to complete it. As it can be seen, the order to follow is marked on its surface.*

III. Results

A first visualization of the data acquired is plotted (Fig. 3.3) and the means and standard deviations are shown in Table 3.1.

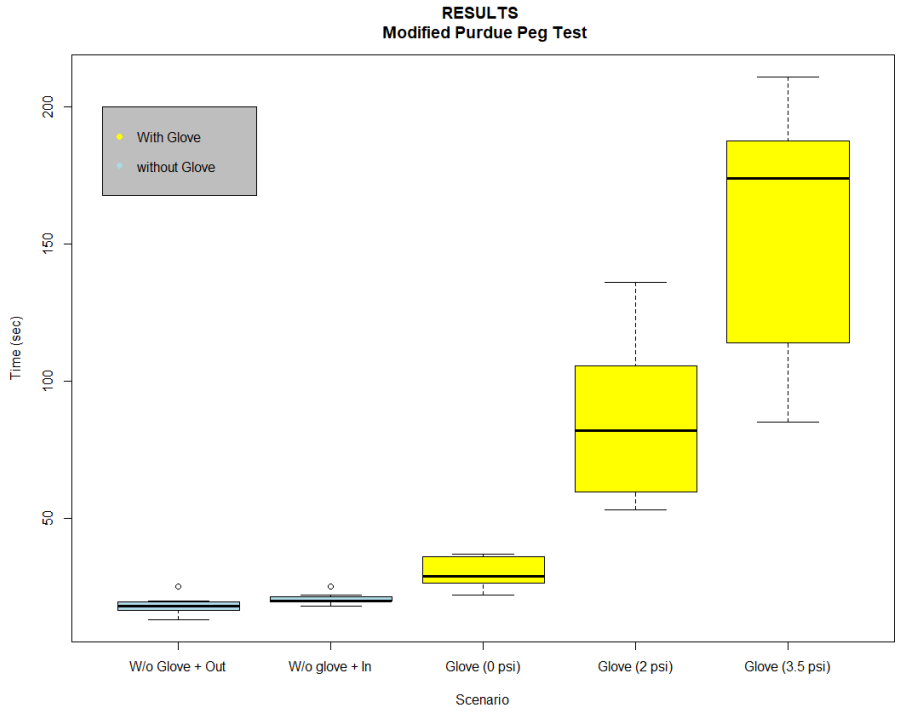

Figure 3.3. Boxplot depicting the amount of time, in seconds, that each subject needed to complete each scenario. *In blue, the barehand scenarios; in yellow, the glove donned scenarios.*

Table 3.1: Sample means and standard deviation of the times to complete the MPPT (seconds) recorded in each scenario, and the global ones.

Scenario	**Mean**	**SD**
Barehand Out	18.3	3.7
Barehand In	20.8	2.2
Glove 0psi	30.4	6.0
Glove 2psi	85.9	31.5
Glove 3.5psi	153.3	48.5
Global	**61.7**	**18.4**

The two Barehand scenarios were compared to see if there is a statistical difference between them. This allowed to determine just a single Baseline scenario. First the homogeneity of variances was checked with a Fligner-Killen test. It was found that the null hypothesis that the variances are the same can't be rejected, thus assuming they are homogeneous ($\alpha = 0.05$, df = 1, p-value = 0.334). With that in mind, a paired t-test with pooled variances was done, and it was found that there was no significant difference between both scenarios (p-value = 0.15).

Therefore, a single baseline scenario was chosen to be the Barehand Out, and the data from Barehand In was not used for analysis. All statistical analysis were then calculated using 4 scenarios: Without Glove Out, Glove 0psi, Glove 2psi, and Glove 3.5psi.

Then, homogeneity of variance of these 4 scenarios was tested with a Fligner-Killeen and it was found that the variances were significantly not homogeneous between scenarios ($\alpha = 0.05$, df = 3, p-value = 0.0157). As the variance was found not to be equal between scenarios, a transformation as is indicated in Eq. 3.1 was used. The new sample distribution can be seen in Figure 3.4. Then, the Fligner-Killeen test was run again, and it confirmed the variances are significantly homogeneous between scenarios ($\alpha = 0.05$, df = 3, p-value = 0.254).

$$Y' = \log(Y) \tag{3.1}$$

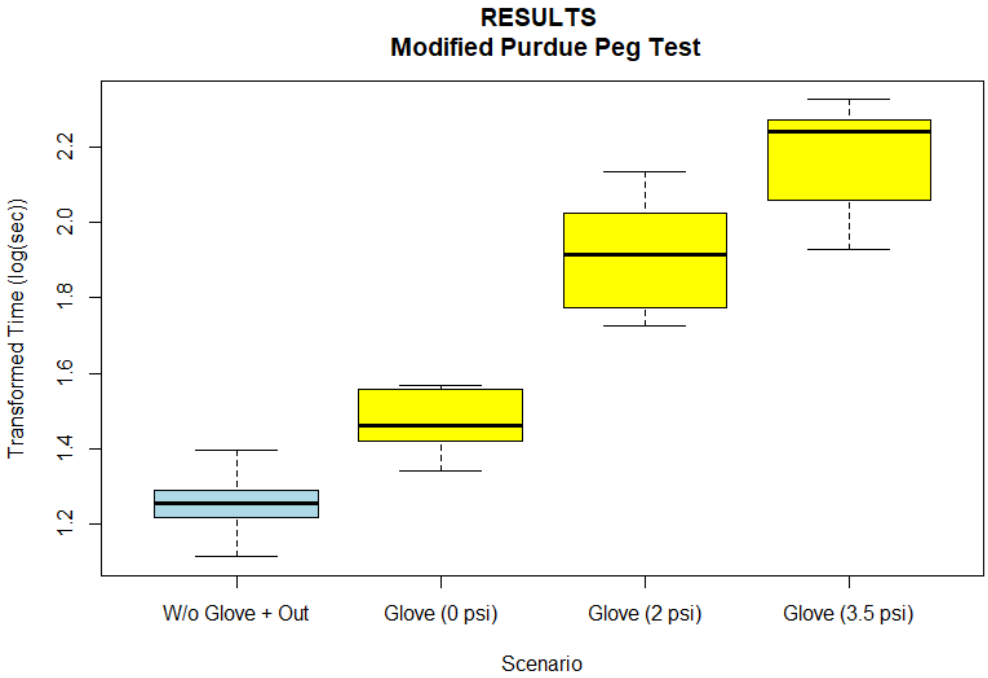

Figure 3.4. Boxplot depicting the amount of transformed time, in log(seconds), that each subject needed to complete each scenario. *In blue, the barehand scenarios; in yellow, the glove donned scenarios.*

To test if the means of the samples between scenarios were equal ($Ho: \mu_i = \mu$), a 1 way repeated measures ANOVA was computed. The test was run on the transformed samples (Table 3.2). The null hypothesis was rejected (Transformed Time: $p < 0.0005$), thus indicating there was a significant difference between conditions. To find which scenarios had their samples significantly different, a series of pairwise comparisons using t-tests with pooled variances were computed, using the

Table 3.2. Results of the 1-way repeated measures ANOVA using the logarithmic transformed times values.

Variation Source	**SS**	**df**	**MS**	**F-value** ***p-value***
Subjects (Block)	0.164	6	0.027	
Between Scenarios	3.560	3	1.187	99.09 *2.21e-11*
Error	0.216	18	0.012	
Total	3.940	27		

transformed logarithmic Times samples. The p-values were adjusted using Bonferroni method. The p-values computed can be seen in Table 3.3. With familywise $\alpha = 0.05$, it was found that all scenarios were significantly different from each other.

As well, a post-hoc Tukey's test was performed parallelly to reassure the trustfulness of the results. It was found statistically significant difference between all scenarios using the transformed data, too.

Table 3.3. Pairwise comparisons results (p-values) using t-tests with pooled SD, with p-values adjusted using Bonferroni. Threshold for significant results is $\alpha = 0.05$.

Scenario	*Barehand Out*	*Glove 0psi*	*Glove 2psi*
Glove 0psi	0.0191	-	-
Glove 2psi	<0.0005	<0.0005	-
Glove 3.5psi	<0.0005	<0.0005	0.0051

IV. Discussion

From the results of the study, different relevant information could be extracted. Recalling that the data was transformed to a logarithmic one, and meaning that all affirmations need to take into consideration that fact before being compared to any other scenario or experiment.

The study was able to confirm the main hypothesis: if pressure is increased, dexterity is significantly decreased (or the time to complete the MPPT is significantly increased) between scenarios. As the pressure increases, it causes the glove to be more rigid, which leads to the increase of the difficulty to perform inter-digital movement. These findings using a pressurized glove are consistent with those reported by Bishu, 1995 [17], who found significant difference between 0psi and 3.2psi using 3 different spacesuit gloves.

However, the relationship between dexterity and spacesuit pressure has been found to be logarithmic. This contrasts with what was hypothesized in our previous study on Hybrid Spacesuits [14], shown in Chapter 2, in which it was considered that the "Mobility" parameter had a linear relation respect to gas-pressure level. That hypothesis was driven by the study made by Mousavi in 2014 [19], in which it was concluded that the required joint torque to bend the proximal interphalangeal (PIP) joint varies linearly with spacesuit glove's pressure. This difference in results might be due not to the fact that the joint chosen to develop the mathematical design trade study was incorrect, as there were other joints reported that were following logarithmic relations, but because in our study it was considered a whole pressurized glove. Also, the glove being used by a human being compared to the single joint being tested with a robotic finger simulator may influence the results. While the robotic finger system may be extremely useful to objectively compare pressurized gloves, it might not be able to take into account all shades of human performance yet. As it was foreseen in Chapter 2, the Mobility parameter of the mathematical model developed there may not be exactly indicative of how a Hybrid Spacesuit would be implemented. The parameter should be revised to incorporate this new found logarithmic relation between dexterity and gas pressure level. As now it was used a high-altitude gas pressurized glove like the one that a Hybrid Spacesuit would use, it can be believed the new logarithmic relation to be more accurate for the Hybrid Spacesuit Concept mathematical design trade study than the logarithmic relations found by Mousavi, who tested individual joints using spacesuit gloves.

On the other hand, most of the subjects (64%, 7 out of 11 subjects) reported different disconformity-related issues. As it can be seen in Figure 3.5, they reported the presence of red-skin in shoulders, wrist, hands and fingers. This was likely due to glove size mismatch and their ability to stand at the glovebox.

Figure 3.5. Some of the red skin reported by subjects.

V. Conclusions and Future Work

The study performed in this chapter was able to prove, through statistical analysis, that its main hypotheses were true. So, it can be considered that:

1. The dexterity tasks are performed significantly different using a pressurized glove at 2psi than at 3.5psi.

   The dexterity tasks are performed significantly different using a pressurized glove at 0psi than at 2psi.

These findings inform the Mobility parameter used in the trade space analysis in Chapter 2. What has been found is that as gas pressure increases, the measures of

dexterity recorded follow a logarithmic function. As it was discussed, this relation may be different to the linear ones found by Mousavi et al. because (1) it was taken into account more complex motions, not only single joins flexions on one plane, and (2) the pressurized glove that was used is considered to be simpler and more flexible than the Orlan spaceglove that they used. Both these conditions considered in this chapter's study are more representative of a proper gas-pressurized element about to be used in a Hybrid Spacesuit. Therefore, it is a better assessment of the GP layer contribution to the hybrid concept.

However, different things will have to be done in in the future to further study this topic and achieve more meaningful results. More parameters (i.e. hand dominance, sex, hand dimensions) should be evaluated, maybe incorporating even more subjects. Should those be tested, the analysis and conclusions derived from the testing would then be able to provide a more global and complete idea on how those effect the relation between dexterity and gas pressure. More knowledge on how those parameters affect the whole suit system will improve the design of the spacesuit.

On the other hand, both the secondary hypotheses were accepted. The conclusions extracted from those hypotheses are:

1. The dexterity tasks are not performed significantly different when performing it inside the glovebox than outside it (p-value = 0.15).
2. The dexterity tasks are performed significantly different when performing it inside the glovebox with the unpressurized glove donned than when they are performed barehand inside the glovebox (p-value = 0.0191).

It can be concluded that using the glovebox to evaluate dexterity is a good enough analogy of a scenario without the dexterity restrictions that the glovebox may have associated. But that the mere presence of the glove, even without being pressurized, directly impacts on the dexterity of the subject.

Additionally, this study provides insight in how using a gas pressurized element not intended for space applications perform under different pressures. Its performance should be compared with EVA-rated elements. This could enable the GP layer of the Hybrid Spacesuit be cheaper and easier to manufacture than current EVA spacesuits. Using a MCP layer, different suit combinations could be assessed to understand better the potential of the GP element in the overall Hybrid Spacesuit architecture. The way the GP layer affects the whole Hybrid Spacesuit may change when being combined with different MCP layer designs. Ideally, the results recorded in this chapter regarding dexterity levels would be much better properly assessed by running different MPPT tests using: (1) only EVA-rated gloves; (2) only MCP glove; (3) EVA-rated gloves combined with MCP gloves; and (4) not-EVA-rated pressurized gloves combined with MCP gloves. With all these results, the advantages (or disadvantages) of the Hybrid Spacesuit concept could be effectively compared with the other existing spacesuit concepts, as the way the GP layer is integrated may have an effect on the spacesuit performance. The design process of the MCP layer should take into consideration the results from this chapter. In the next chapter, the conceptual development of the MCP layer will be discussed.

Chapter 4

Study on the Mechanical Counterpressure Components of the Hybrid Spacesuit

I. Introduction

This chapter will demonstrate how tools to facilitate the design and manufacturing of a mechanical counterpressure (MCP) glove were developed. Such a glove would be integrated with the GP glove from Chapter 3, conforming a fully operable Hybrid Spacesuit glove. The glove is the ideal testbed for MCP development due to its small radius of curvature compared to other parts of the body, its inherent geometric variety between hand-parts, and its high-mobility capabilities. If successful, the technology developed here could be quickly escalated to the other parts of a full-body garment.

The chapter will start with an analysis of off-the-shelve fabric materials. Following the creation of this library of fabric properties, a sizing tool is created to automatically generate a glove pattern from hand geometry. Then, the pattern is used to guide the design of a full MCP glove, which requires additional design accommodations discussed herein.

The work shown in this chapter was developed with the collaboration of Andrew S. Kerr, who helped conduct the fabrics' analysis and was the main responsible of coding the sizing tool.

II. Materials Evaluation

A. Governing Principles behind MCP

Before starting the design and prototype of MCP gloves, it was needed to understand which materials were at our disposal, as the main actuator of a MCP garment is its elastic restrain layer. This layer applies the required pressure to the body. If the MCP element is modeled as a thin walled pressure vessel (Figure 4.1, [28]), in which the internal pressure is the pressure applied to the human body, the hoop stress equation (Equation 4.1) can be used to calculate the load being produced [12], [28], [31].

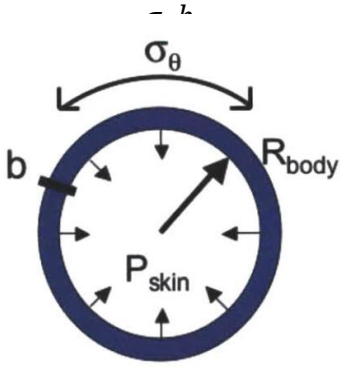

Figure 4.1. Definition of variables for a MCP garment cross section. *The garment is modeled as a thin walled pressure vessel. Reproduced with permission of Anderson [28].*

The equation takes into account the thickness of the material (b), the radius of the body to which the garment applies the pressure (R_{body}), and the circumferential hoop stress (σ_θ) to find the pressure that is being applied against the body (P_{skin}). This holds for any surface radius of curvature, until the point of flat or concave surfaces,

which can be found on the hand. This is the case for the palm of the hand, which has a concave shape with a huge radius of curvature compared to the radius of the fingers.

In this chapter, a 2psi MCP garment is the design target. Note also that the thickness of the material scales linearly with pressure, but inhibits tactility, which is undesirable.

Another point to take into consideration before choosing the best material is its performance under elongation. Each fabric has a different strain-stress behavior. Different factors have a direct effect on this behavior. The three main ones are: the tensile force that its threads are able to sustain; the way they have been woven (and if it is an isotropic or anisotropic material); and the direction under which the force is being applied to the fabric (on the warp or the weft). The MIT Bio-Suit™ hypothesized that the ideal fiber for their "second skin" should follow a curve like the one depicted in Figure 4.2 [37]. The three main zones they detected were:

1. An extremely elastic start (the first 5% stretching), to allow donning and doffing and an easy adaptation of the fabric to small skin discontinuities (green area in Figure 4.2).
2. An operating range that should be between the 30% and the 70% stretching of the fabric (blue area in Figure 4.2). This would allow the user to move and bend the fabric without creating too many discontinuities in the pressure surface. All body parts under pressure that are moved would continuously receive the same uniform mechanical pressure, which they desired to be 4.3psi like the current pressure used in EMU spacesuits.

3. A failure point of the fabric not before reaching the double of the operating pressure, taking into consideration a factor safety of 2 (red area in Figure 4.2).

Although a material that exactly acts like that has not yet been identified, this graph, and the logic behind it, helps to determine which are the characteristics that should be considered when choosing which fabrics to use in the MCP layer of the hybrid glove.

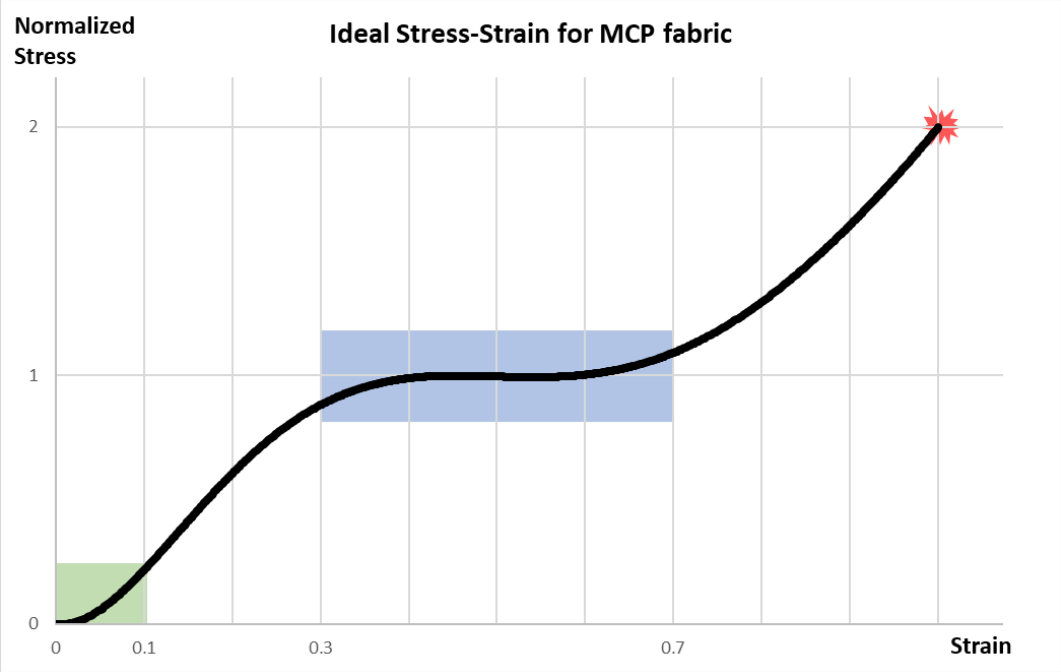

Figure 4.2. Ideal force Displacement Curve for MCP fabrics. *Theoretical approximate stress-strain curve of the ideal MCP fabric. Inspired by the "Ideal Force-Displacement Curve for Bio-Suit Fiber" [37]*

B. Testing Method

After screening for possible fabric candidates [38], and taken into consideration the materials used in other MCP projects [10], [27], [39], [40], as well as the materials currently being used in the EMU spacesuit [41], a total of 9 materials were purchased

and tested. To get their mechanical properties, a 5900-S Instron was used. The samples that were used measured 2.5cm x 10 cm. Each sample had two zones sizing 2.5cm x 2.5 cm on the sides that served as grip points with the Instron (Figure 4.3). Three replicate samples were cut from each fabric, and a stress-strain curve was computed from each. The test terminated when the sample reached its breaking point. The mean curve of the samples was used for further fabric analysis for our MCP glove.

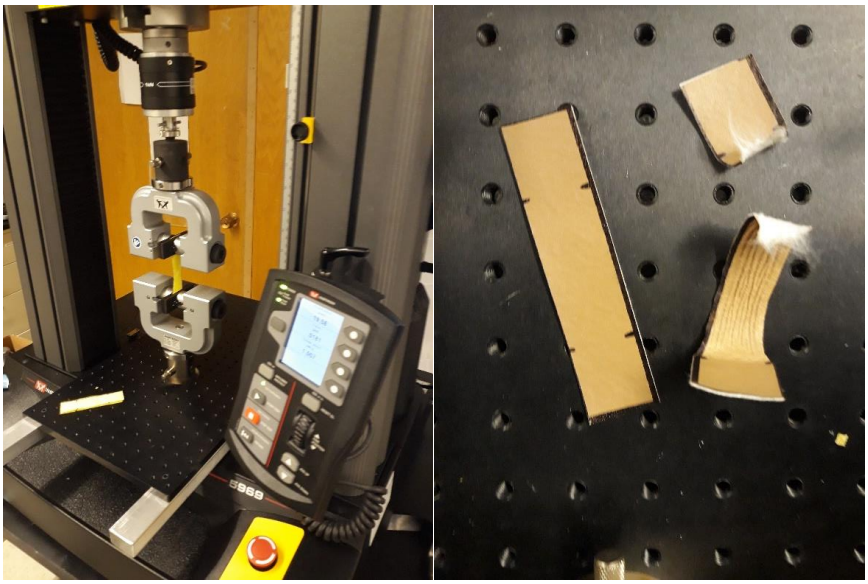

Figure 4.3. Stress-Strain experiment on the Instron. *On the left image, the Instron can be seen how it is recording data from a loaded fabric sample. On the right image, a fabric sample (2.5x10cm) with the grip places marked (2.5x2.5cm) can be seen before being loaded into the Instron (left) and after it has achieved its breaking point and has been unloaded from the Instron (right).*

C. Results

All the samples that were analyzed are shown in Appendix 2. For each fabric has its own plot, showing the three recorded tests and the mean curve of those. Also, the direction over which the force was applied is recorded (warp, weft, or isotropic). The thickness of the material is recorded, too. An example stress strain curve can be seen in Figure 4.4.

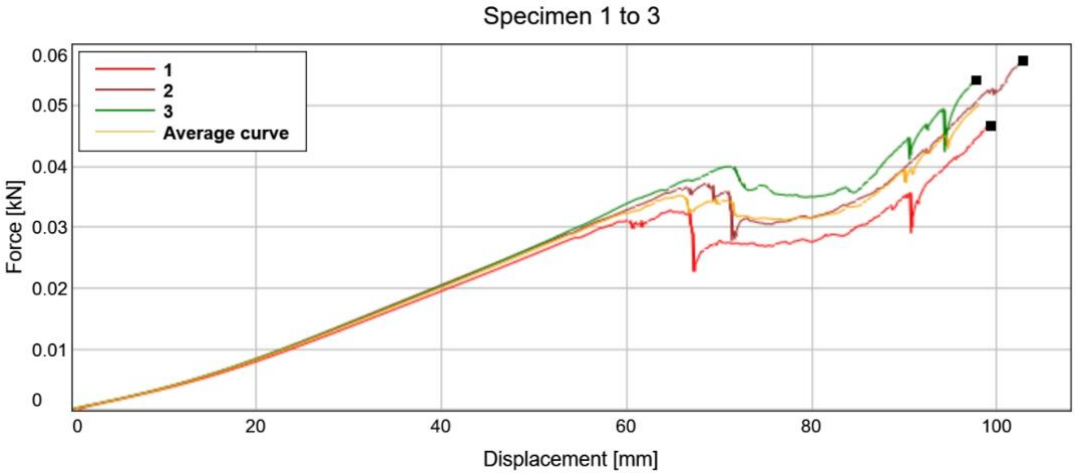

Figure 4.4. Wetsuit Neoprene. *Isotropic orientation. Thickness of 0.0266 cm.*

D. Discussion

From all materials tested, the best for our MCP design is the Wetsuit Neoprene (Figure 4.4), as it is not thick, and, from its stress-strain curve, it can provide effectively our desired pressure. This neoprene is composed by two layers: a thick one that is the neoprene foam, and a cover layer made out of spandex in just one side. This is why two break points appear in Figure 4.4. The spandex side is much smoother than the other, so it will face the inner part of the glove to facilitate donning and doffing. The other ones can be classified in three different groups:

1. **Too much force is required for little displacement:** Neoprene Rubber, Heavy Duty Cotton, and Vynil.
2. **Too much displacement is required to apply too little compressive force:** Foam-backed Headliner, Ryon, Suplex, Cotton lycra
3. **Inelasticity sets the breaking point at a small strain:** Heavy Duty Cotton, Cotton cozy flannel.

III. Pattern Sizing

Once the fabrics' intrinsic properties were recorded, a sizing tool was developed to automate the way the pattern for the MCP layer of the Hybrid Spacesuit glove is designed. The motivation was to create a standard and subject specific way to design the elastic restrain layer of the MCP glove.

The tool was coded using MATLAB [32]. The steps that the tool follows to size the pattern are (Appendix 2):

1. The three stress-strain curves recorded by the Instron are loaded by the program. With this information, the mean curve is extracted.
2. The desired MCP pressure is then input. In our case, it was set to be 2 psi.
3. Once plotted, the software changes the variables of the curve to Strain, using Equation 4.2 where ε is the strain, ΔL is the previously computed displacement, and Lo is the initial length of the sample (5 cm in our case), and Effective Stress, which is a variable already given by the Instron that takes into account its area profile. The result can be seen in Figure 4.5.

$$\varepsilon = \Delta L / L_0 \tag{4.2}$$

4. Now, considering a Poisson ratio of 0.5, we take into account the fact that the more pressure the fabric applies, the more stretched is. To compute the thickness, Equation 4.3 is used, where b is the thickness of the material, b_o is the initial thickness of the fabric (2.66 mm in the

wetsuit neoprene case), 0.5 is the chosen Poisson ratio, and ε is the strain associated to a specific stress. This will help to better understand the thickness of the material when applying a specific desired pressure (Figure 4.6).

$$b = b_0 - b_0\,(0.5\,\varepsilon) \tag{4.3}$$

5. Then, it is computed the relation between the radius of curvature and the fabric strain for our set pressure (2psi). This relation can be seen in Figure 4.7. The equation behind it is the already stated hoop stress equation (Equation 4.1).
6. The output is 50% of the theoretical circumference required to achieve 2 psi (Initial Required Half Circumference, Figure 4.8). This is done because the glove pattern is comprised by two same pieces of fabric.

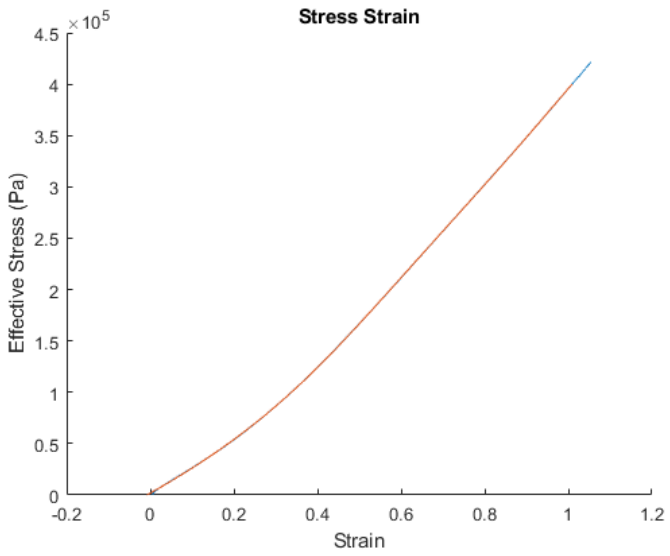

Figure 4.5. Fabric Stress-Strain Curve. *The effective stress, in Pa, is plotted against the Strain, in a normalized percentage.*

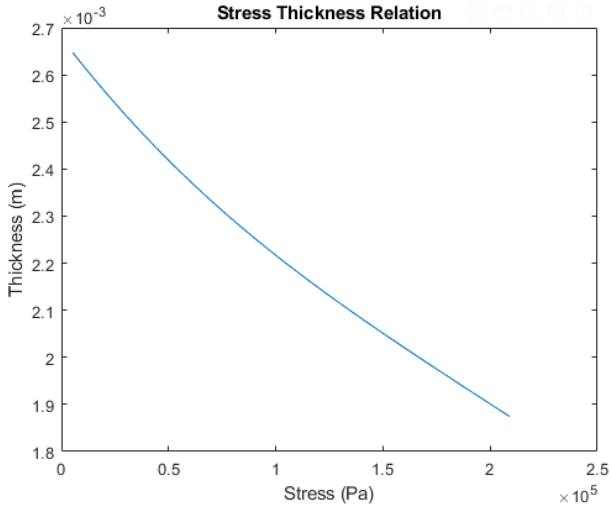

Figure 4.6. Fabric Thickness and Stress relation. *Considering the applied effective stress, related to a certain displacement, the thickness of the fabric is computed considering a Poisson ratio of 0.5.*

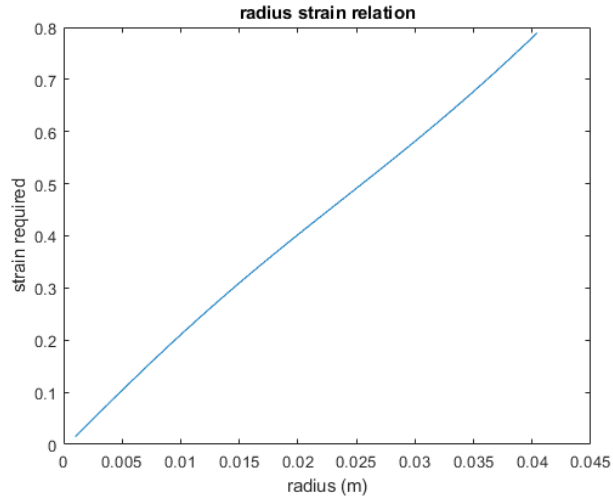

Figure 4.7. Circumference radius relation with Fabric Strain. *The computation uses the hoop stress equation considering a set 2psi as desired internal pressure.*

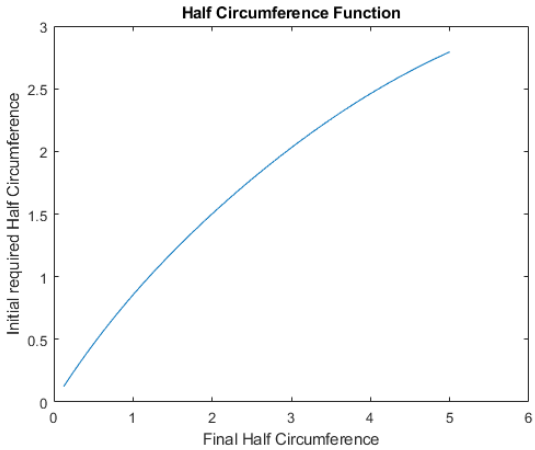

Figure 4.8. Half Circumference Function. *Final Half Circumference states the half of the perimeter of a circular body part, and the Initial Required Half Circumference states the length that each side of the glove pattern should have to be able to apply 2 psi using the Wetsuit neoprene in this case. Variables computed in cm.*

SolidWorks [42] was used to design our MCP glove pattern. As it can be seen in Figure 4.9, multiple hand dimensions are taken, and each variable is independent of the others, so the design can be adapted to each user. The output from the code (Figure 4.9) is used to properly size the thickness of the fingers' parts. Conversely, the length of the fingers was measured to the person and put unvaried on the pattern.

The resulting MCP glove pattern can be seen in Figure 4.10. A laser cuter was used to achieve a high precision cut of the pattern, as it can be seen in Figure 4.11.

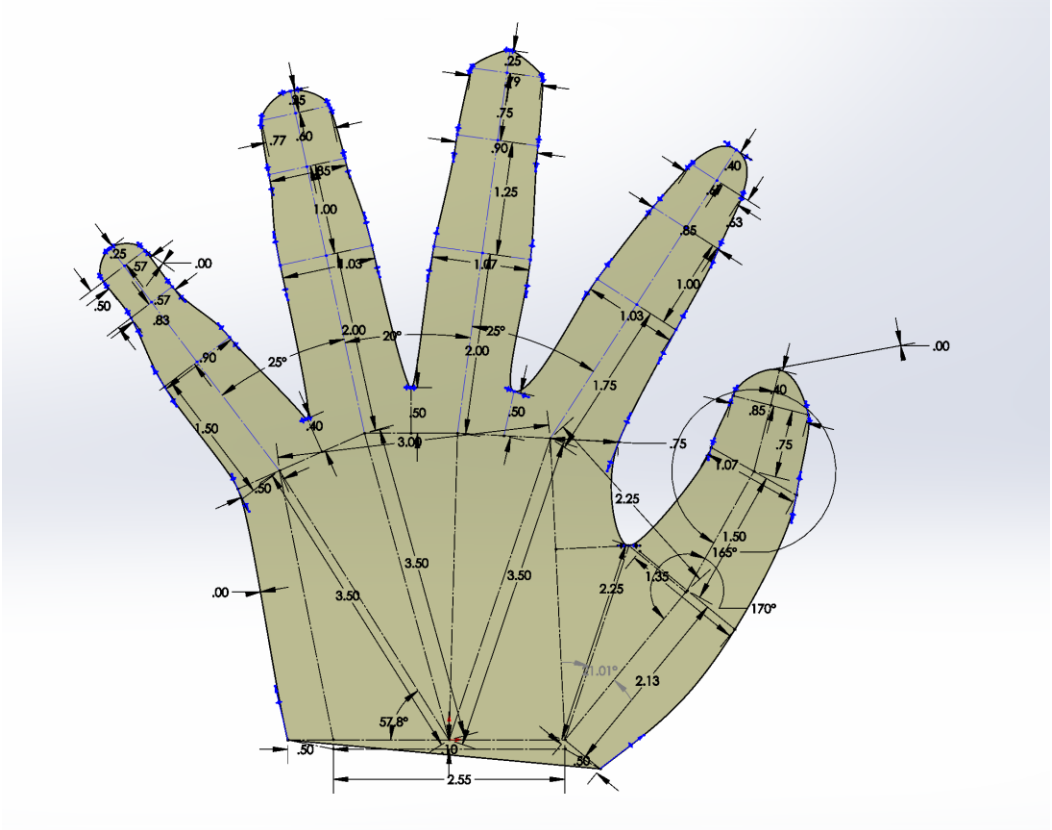

Figure 4.9. Glove Pattern Design. *The across fingers values come from the Half Circumference Function. The other values, such as length of the fingers, are measured directly from the user.*

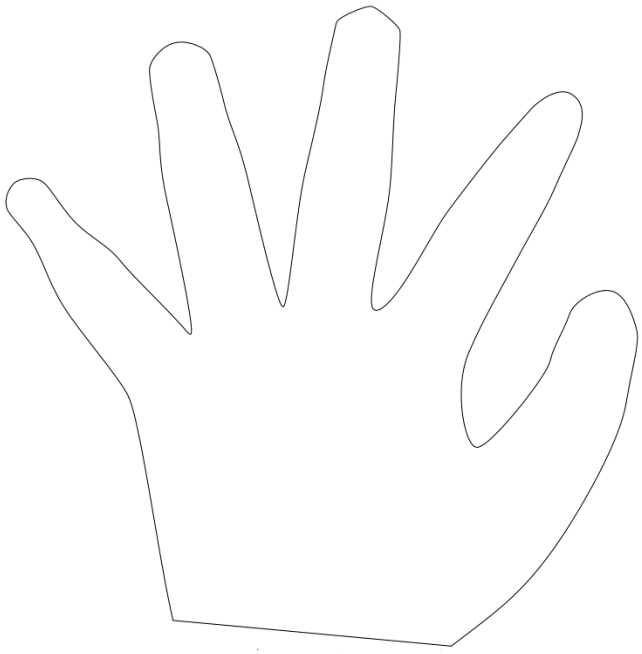

Figure 4.10. Glove Pattern Ready to Print. *This file is ready to be loaded into a laser cuter.*

Figure 4.11. Laser cut paper with the MCP pattern. *The fabric behind it is the Wetsuit Neoprene that is intended to be used for the MCP glove restrain layer.*

IV. MCP Glove Architecture Design

The architecture was determined through an iterative design process. During this work, each week a new iteration was manufactured and tested, serving as a baseline for the next iteration that was about to be done for the following week. The iteration progression of the MCP glove design is presented in 3 main subsections. Each subsection corresponds to the 3 elements that, together, comprise our MCP glove design:

1. Elastic Restrain Layer
2. Palm Pressure Distributor
3. Anchoring Gauntlet

The Elastic Restrain Layer (ERL) applies the pressure. While in some places it is easy to perfectly apply the theorized pressure thanks to their small radius of curvature (fingers), other places it is not possible achieve pressure with the elastics (palm). To solve this problem to transmit enough pressure to the palm of the hand a Palm Pressure Distributor (PPD) was designed to transmit the elastic pressure from the ERL to the palm concavity using an ergonomically engineered design. To ensure the proper placement of these elements, a third component was designed. This is the Anchoring Gauntlet (AG), which provides an anchorage point to the whole MCP glove, ensures proper finger fit, and helps apply enough pressure on the PPD (and so to the hand's palm).

A. Elastic Restrain Layer

i. Design Concept

The Elastic Restrain Layer (ERL) is intended to be the main pressure actuator of the system and is cut using the pattern previously developed from the Wetsuit Neoprene fabric. Two mirrored layers are cut. No seam allowance was required (1) to ensure no fabric overlap (which would cause a pressure discontinuity) and (2) not to have threads on the inner part of the glove, as those would likely cause skin injuries due to the tightness and the pressure being applied to the hand.

ii. Iterations

Initial prototypes used to investigate sizing were made from Rayon fabric, as it is cheaper and easier to sew. With the paper pattern, two sides of the glove were cut and sewed together, ensuring that, although an overlapping seam was present, the inner layer of the glove was identical to the pattern. The result of this first iteration can be seen in Figures 4.12 and 4.13. As it can be seen in Figure 4.12, two different gloves were manufactured. The first prototype (marked with an N, for Normal) was used to test if the hand measurements inputted in the SolidWorks design matched with the real hand once the glove was sewed.

From this first prototype, the effect that an inner seam with visible thread has on the skin was reported as red marks. The glove pattern, although presenting wrinkles in the lower part of the fingers, was considered fit enough. Although the material was not the Wetsuit Neoprene, pressure on the hand was already experienced.

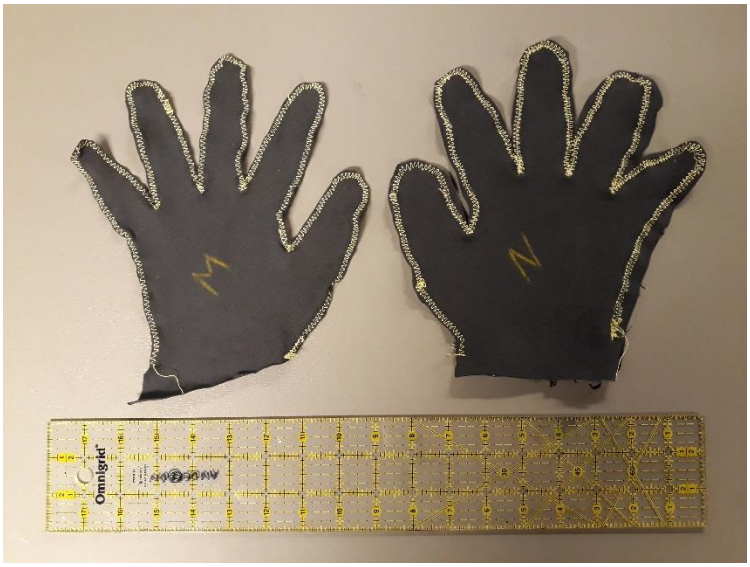

Figure 4.12. Elastic Restrain Layer v1. *The M model is the one done with a pattern that takes into consideration the MCP sizing. The model N is the one that doesn't have any MCP consideration, and was used to prove the anthropometry of the glove pattern*

Figure 4.13. Elastic Restrain Layer v1 donned. *The overlapping seam can be seen on the contour in yellow, as a Kevlar based thread was used.*

A prototype was then manufactured from the Wetsuit Neoprene fabric. However, it was not the same fabric as the one tested during previous section II.A, as that one was reserved for latter iterations. Instead, a cheaper and thicker neoprene, provided by OceanFirst scuba diving shop, was used. By using that other neoprene fabric, it

was wanted to get a better understanding in how to properly manipulate neoprene. This material was thicker (5 mm instead of 2.66mm) and had two layers covering the neoprene material, one side having a spandex layer, facing the inner side of the glove, and the other side an impermeable paint layer, facing the outer side of the glove (Figure 4.14).

Figure 4.14. Thicker Wetsuit Neoprene. *The two specular sides of the glove are depicted, showing that in for this material the neoprene side covered by spandex (in black) faces the inner part of the glove while the neoprene side covered with impermeable paint (in light grey) faces the exterior.*

To manufacture the neoprene prototype, wetsuit manufacturing techniques were used. The "blind stitch" was used and sewed by hand (Figure 4.15). It enables us to sew a material having visible threads in just one side of the fabric (the outer one in our case). A polyester thread was used because it had more elasticity (Figure 4.16).

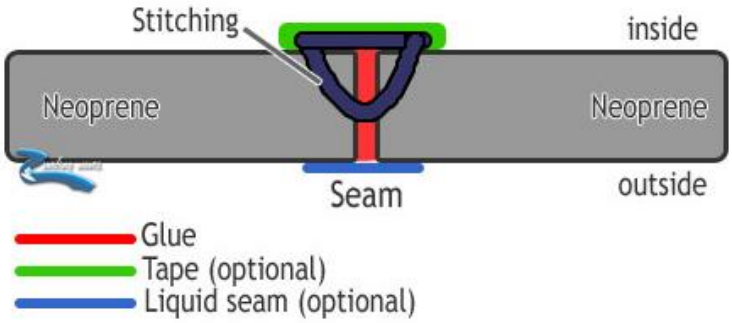

Figure 4.15. Blind Stitch Schematic. *From surfing-waves.com.*

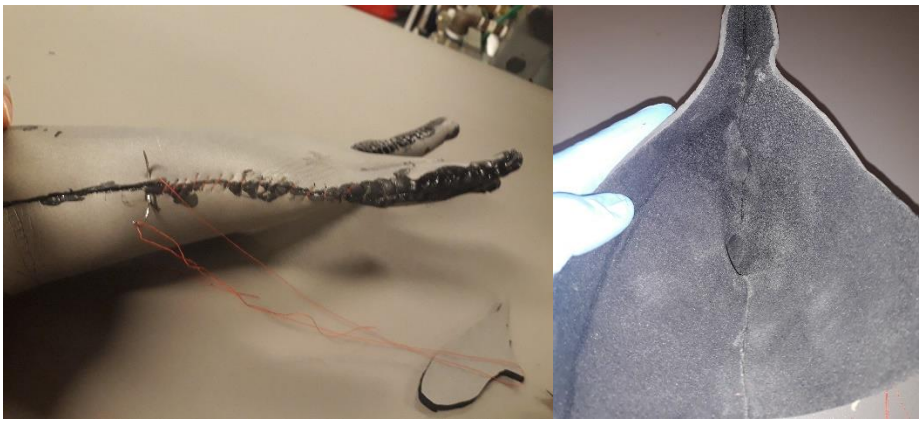

Figure 4.16. Blind Stitch Used. *On the left, the curved needle and the red polyester based thread can be seen in the middle of the blind stitch process. In contrast to the left image, in the right one, which depicts the interior of the glove, it can't be seen any red thread, just flat neoprene layers.*

The process to manufacture this second version of the ERL, was as it follows:

1. Two layers of the Thick Neoprene Wetsuit fabric was cut following the MCP paper pattern.
2. The layers were glued together using a Neoprene Cement, which firmly bonded the sides of the neoprene fabric.
3. A curved needle was used to blind stitch the neoprene, thus enhancing the bond and ensuring a better structural stability of the system.
4. A second layer of the Neoprene Cement was applied over the seam, to fill the holes created around the thread insertion points.
5. A silicone-based resin was poured over the seam to improve its stability as well as the stitch's holes. Also, it had impermeable properties.

The final result of this iteration can be seen in figure 4.17.

This second iteration provided many insights. The blind stitch was slow to implement but was ideal to bond the two neoprene layers while the neoprene cement was drying. Further, the user cannot feel any of the threads when donned. The

polyester-based thread also showed better results than the Kevlar one (Figure 4.13 in yellow), as it was structurally more stable. The Kevlar thread sometimes acted like wool and unraveled. The Neoprene cement created bonds that were strong and flexible. Once, a rudimentary stress test was performed on the cemented bond, and the neoprene didn't break through the cement union, but through the fabric on its side (Figure 4.18).

Figure 4.17. Elastic Restrain Layer v2. *The left image it can be seen how the silicone-based layer (in white) is drying. The right image the final result can be seen.*

Figure 4.18. Neoprene Cement Break-Stress test. *As it can be seen, the fabric breaks along the bond, but not through it (black arrow). Also, the elasticity of the neoprene cement that was used is marked by the white arrow.*

Design improvements were also identified. The silicone-based resin was unable to bond to the neoprene and started to peel off soon after being cured. It was also difficult to create the finger tips. As seen in the middle finger of the Figure 4.17, the finger tips made the seam line rotate nearly 90° with respect to the other fingers. Also, although the blind stitch seemed successful, it was detected that its proper implementation was extremely dependent to the thickness of the neoprene.

Before starting the 3rd iteration, it was checked if the blind stitch could be used in the final Wetsuit Neoprene (2.66 mm thickness). It was found that instead of helping to bond the layers, the hole created by the needle destabilized the fabric, causing the appearance of bigger holes and cuts. So the blind-stitch technique was then not used in the 3rd iteration, and the bonding was relied solely on the neoprene cement. A final iteration (v3) of the ERL was manufactured. The Wetsuit Neoprene used to design the glove pattern was cut using the paper patterns, with special care at the fingertips, to facilitate the donning and doffing. The side with a spandex layer on it would face inward (Figure 4.19).

Figure 4.19. Definitive Neoprene Wetsuide Pattern cut. *The darkest side corresponds to the inner side of the MCP glove, as it is covered by spandex, which facilitates donning and doffing.*

The neoprene cement was applied progressively 5 cm at a time to ensure a good bond. Two coats were used. The cement required 5 minutes to dry, then a second layer was applied. Finally, both glued sides could be compressed together, creating a strong but flexible neoprene bond. In Figure 4.20 the neoprene cement application process is depicted.

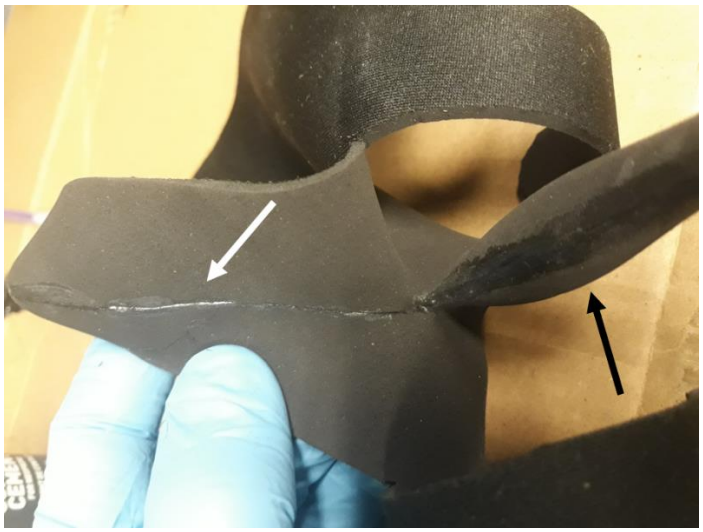

Figure 4.20. Neoprene Cement Application. *The white arrow signals how the neoprene bond looked when the cement had cured uniting both neoprene layers. The black arrow signals a part of the glove that had already received the covering neoprene cement layer.*

Once all the glove perimeter was bonded, a second layer of neoprene cement was applied over the bond to ensure that no holes were left. Also, some neoprene ripped off parts where detected (due to scratching with some pointed elements), and were as well treated with neoprene cement (Figure 4.21). The final ERL is shown in Figure 4.22 donned.

Figure 4.21. Torn Neoprene Amendment. *The neoprene was a little teared in the middle of the palm of the glove. A neoprene cement layer was applied to it to avoid its expansion and final breakage.*

Figure 4.22. Elastic Restrain Layer v3. *Without any thread used, the ERLv3 achieves the desired design characteristics, as it is completely flat in its inner side, has the exact coded pattern shape and applies a strong pressure on the fingers and most parts of the hand of its user.*

B. Palm Pressure Distributor

i. Design Concept

To address the problem of the concavity of the hand a palm pressure distributor (PPD) is envisioned. This subsystem should be capable to transmit the circumferential pressure applied by the ERL to the inner part of the palm in a uniform and adaptative way, that could enable free hand movement, as well as a good interaction with physical objects.

The idea with which it was decided to proceed was a semiflexible element with a user-specific convex shape that had to be placed in the palm of the hand.

ii. Iterations

The material chosen to be used for the PPD was silicone. (Figure 4.23). Using a mold of the hand, it was decided that the PPD should have a convex shape with its boundaries set on the palm creases. This enables free hand movement, particularly for thumb abduction/adduction which is critical for normal hand movement. The first iteration of the PPD cut this region from the silicone hand mold, as it can be seen in Figure 4.24.

This PPD iteration identified that the hand can't be placed on a liquid silicone surface, because (1) it is easy for air to get stuck between the hand palmar concavity and the silicone (as it can be easily seen in the center of Figures 4.23 and 4.24), causing undesired surface discontinuities, and (2) the convex shape on the side distal to the palm can't be achieved in that manufacturing process. If the ERL side is flat,

the concavity of the hand is just partially corrected: it doesn't have a convex profile, needed so the elastic pressure can be applied.

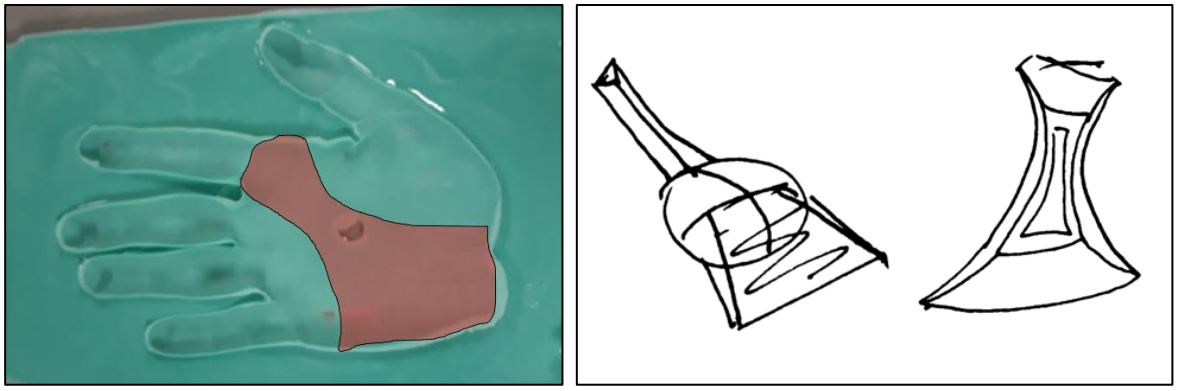

Figure 4.23. Silicone Hand Mold. *A whole mold of the hand was done using silicone to help identify how the PPD should look, identifying the boundaries it should have with respect to the hand palmar creases. A quick sketch of the chosen PPD shape can be seen overlaid in red and the drawn concept depicted on the right.*

Figure 4.24. Palmar Pressure Distributor v1. *The silicone hand mold is cut (left) and placed under the ERL, along a belt to help fix it on the palm.*

The second iteration of the PPD was manufactured differed significally. A putty dough was used to create a more convex-shaped PPD for the outermold line, (Figure 4.25). This putty dough, after being shaped, is used to create a plaster mold. This plaster mold is then cutted in half and filled with silicone, as it can be seen in Figure 4.26.

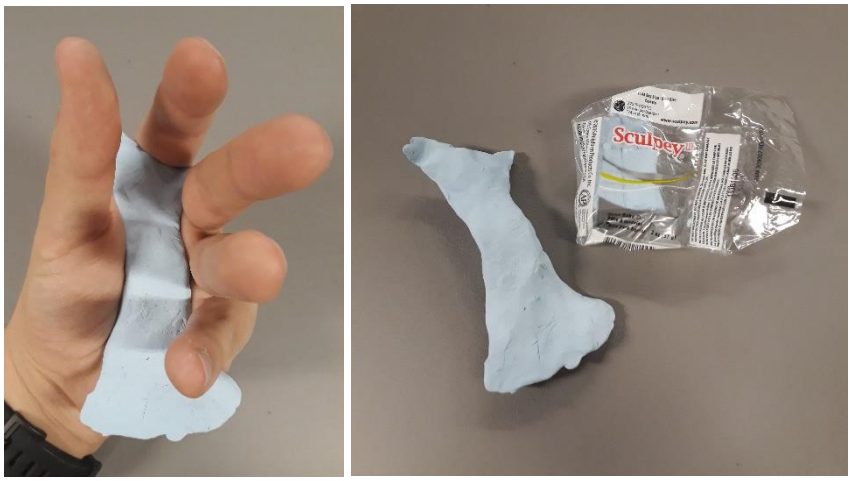

Figure 4.25. PPD Putty Dough Model. *The putty dough allows for quick prototyping and to easily modify the shape of the PPD model. The dough was not dried, as it is needed to be flexible to be able to be pulled out from the plaster mold*

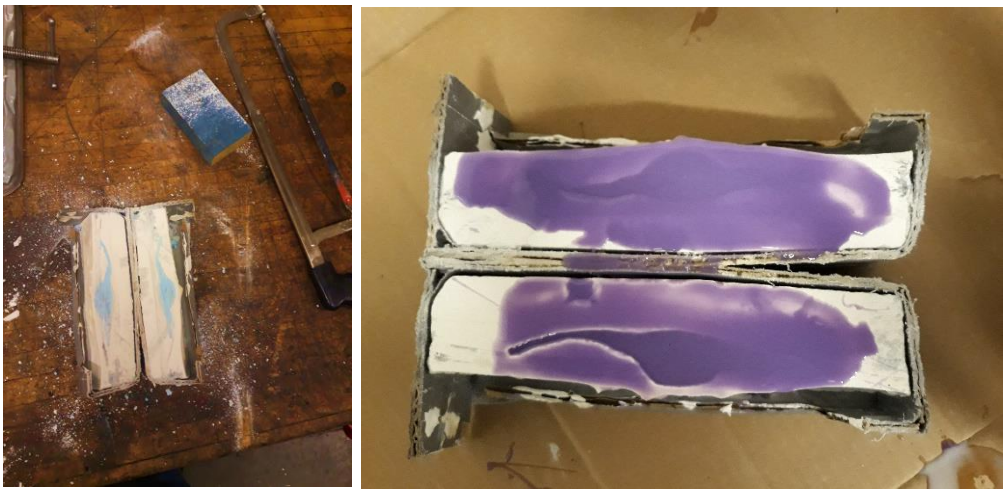

Figure 4.26. PPD Plaster Molt. *On the left, the plaster model can be seen how has been cut in half with still the putty dough model still in it. On the right, the plaster mold has been emptied and filled with silicone.*

Once the poured silicone is cured and pulled out from the plaster mold, the two silicone PPD halves are united using more silicone, thus finishing the second iteration (Figure 4.27).

This iteration was the proper convex shape was achieved along with a highly ergonomic profile. Before this iteration, it was considered that the boundaries of the PPD had to be set to on the palmar creases. However, after trying to combine the PPD

with the ERL, it was found that these boundaries created a discontinuity line in the pressure distribution on the palm. This was the cause of different red skin marks, as well as improper continuous pressure over the palm of the hand.

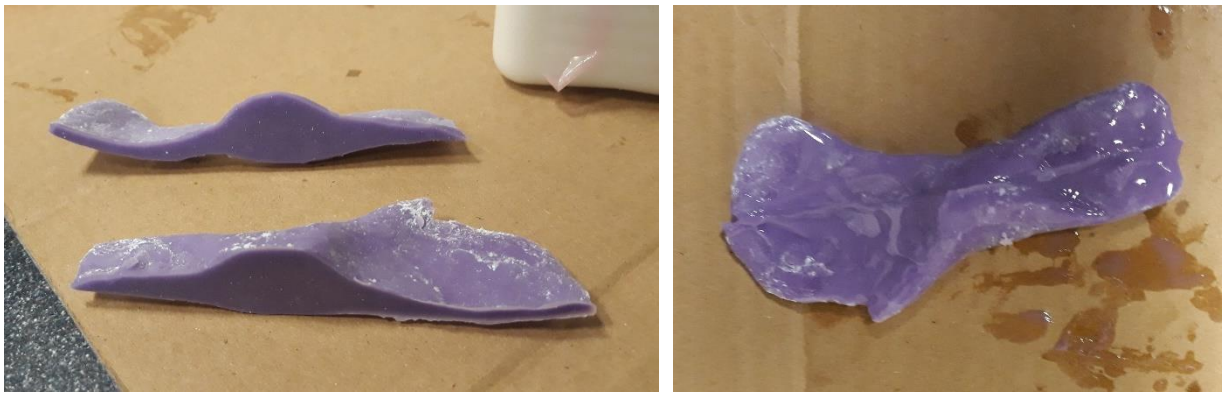

Figure 4.27. Palmar Pressure Distributor v2. *The two silicone halves are united using more silicone to create the second iteration of the PPD.*

To correct that, the third and last iteration aimed to give the PPD a more palmar uniform and continuous shape, without renouncing to the grip capabilities of the palm. This was achieved by extending the silicone area on the palmar side of the PPD. Also, two longitudinal cuts were performed on the ERL side to enable a better moved of the hand, as they facilitate the gripping movement. These changes can be seen in Figure 4.28 signaled by the white arrows.

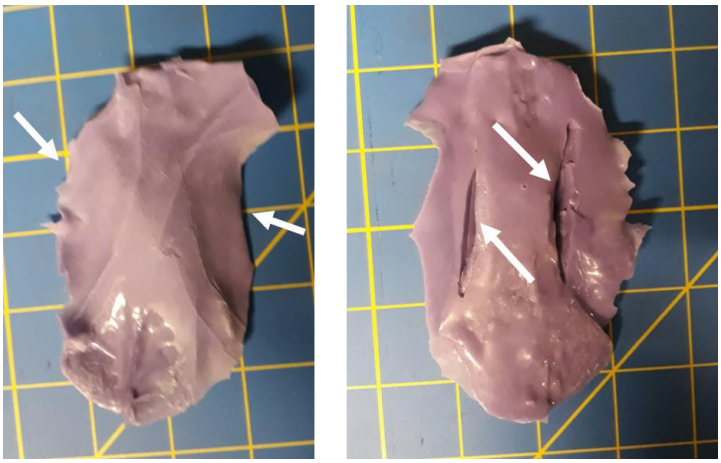

Figure 4.28. Palmar Pressure Distributor v3. *Left image corresponds to the palm side of the PPD. Right image corresponds to the ERL side, with the two cuts that enable the grip movement of the hand.*

C. Anchoring Gauntlet

i. Design Concept

A system had to be developed to ensure that the ERL and PPD were placed in their correct positions with respect to the hand while performing manual activities. This would be similar to the ones developed before [18], [27], [43] . The third subsystem of this glove is the Anchoring Gauntlet (AG). The AG has two functions that drove its design: (1) provide and anchoring point to all the system of the MCP glove, and (2) apply extra pressure over the hand.

ii. Iterations

Three main areas where to use anchor points and apply pressure were identified: around the thumb, around the PPD, and over the zone immediately under the little, ring, and middle fingers. These three areas corresponded to the 3 palmar hand zones that are separated by palm's creases. The placement of these first three restraints can be seen in Figure 4.29. The restraints, belt-mechanisms, are sewed over a small gauntlet manufactured using the previously designed "Normal" glove pattern, but without any fabric nor seams on the fingers.

The anchoring point for any restrain belt should be in the back of the hand, as it is one of the bigger available surfaces to mount to. A small gauntlet was sewn using spandex and the "Normal" glove pattern, and a synthetic inelastic fabric was sewed in its reverse. This inelastic fabric was used as the first anchoring point. Two different systems were sewn on it. The first one was a set of 4 interdigital elastic bands. These were intended to help in the donning and doffing process of the MCP glove, as well as

Figure 4.29. Anchoring Gauntlet Preliminary Study Concept. *In the left image, the three restraints can be seen over the hand, sewed to the external gauntlet (with red thread). On the right, proof that they allow good finger and palmar movement.*

helping the ERL to be fixed between the fingers, as this is a common place were pressure discontinuities may appear. The second system was a leather belt, which purpose was to help apply pressure on the PPD. This belt, instead of being sewn on the inelastic fabric, it was sewn on the palmar side of the gauntlet. As it can be seen in Figure 4.30, two different types of anchoring were tested: a single and a double anchoring seam.

Figure 4.30. Study on the Palmar Central Restrain Anchoring. *Two point seam in the left image. Single point anchoring seam in the right image.*

The resulting first version of the Anchoring Gauntlet can be seen in Figure 4.31. This system was tested for 60 minutes. Red skin on the palmar side of the metacarpal-phalange (MC-P) joints were found, as it can be seen in Figure 4.32. This was identified as a primary issue to resolve for subsequent iterations.

Figure 4.31. Anchoring Gauntlet v1. *The inelastic white fabric can be seen sewed on the reverse side of the gauntlet, with the interdigital restraints already donned between the fingers. The brown leather belt restrain can be also appreciated in the image. The right image shows how the profile of the system looks like when the PPD is incorporated.*

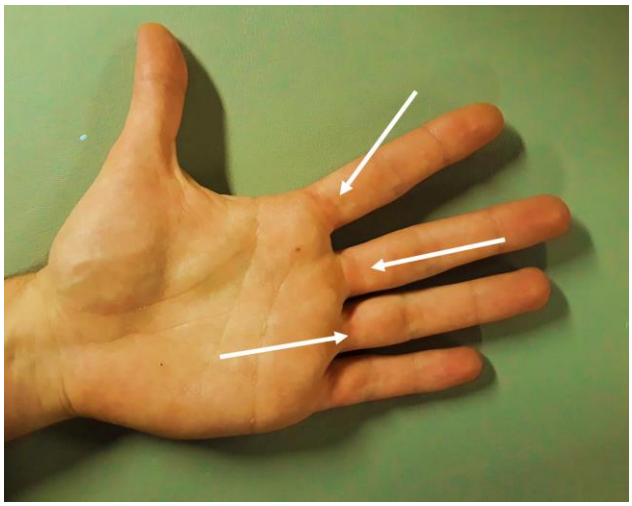

Figure 4.32. Red Skin marks due to the AGv1. *Signaled by black arrows, the red skin marks can be seen in the MC-P joints, indicating that a possible restriction in blood circulation may happen due to the interdigital elastic restraints.*

The second iteration of the AG improved anchoring by being positioned on the wrist with Velcro. The leather belt was replaced by an inelastic synthetic material sewn to the gauntlet in two different points on the palm side. It was also secured with Velcro. The interdigital elastic bands were sewed to the center restraint. However, in this iteration, instead of having a loop shape, they were just linear straps connected to a solid plastic square on the back of the hand. This was tied with a Velcro band to the main anchoring wrist element. The interdigital restraint uses a "click-and-go" mechanism, facilitating the donning and the doffing.

All these different elements can be seen acting together as the AG v2 in Figure 4.33.

Figure 4.33. Anchoring Gauntlet v2. *The AGv2 appears donned with the ERLv1 and the PPD in it.*

The final iteration of the AG improved the poorly shaped plastic square that was part of the interdigital donning-doffing system. Instead, a new piece was designed for this specific job. This modelled piece was 3D printed using PLA, and then sewed into place in the AG. This ensured a better stability of this restrain subsystem.

The model and the printing process of this specific piece can be seen in Figure 4.34, and the last and definitive AG model is displayed in Figure 4.35.

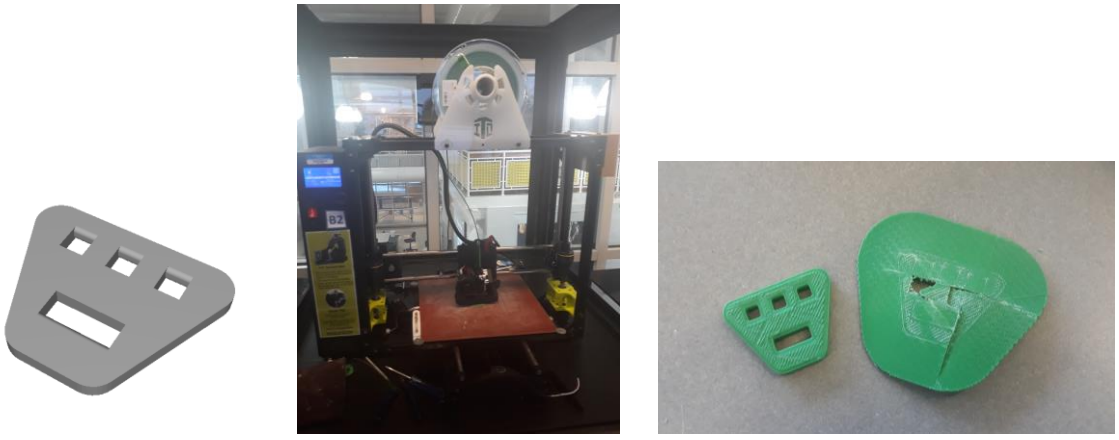

Figure 4.34. 3D Printing of the Interdigital Restrain Element.*The left image shows the model in the SolidWorks environment. The center image shows how the piece is being printed using PLA in the ITLL services in CU Boulder. The right image shows the final printed element.*

Figure 4.35. Anchoring Gauntlet v3. *All elements have been integrated, including the 3D printed element.*

D. MCP Layer Final Design

After having iterated each subsystem at least 3 times each, the three systems were combined and fully integrated in a single MCP glove, which can be seen in Figure 4.36. This MCP glove is intended to help set the baseline from which to progress towards a more definitive design version that can be integrated as the MCP layer on a full Hybrid Spacesuit glove.

Figure 4.36. Final MCP Glove design. *The three subsystems (ERL, PPD, and AG) have been integrated in this final version of the MCP Glove.*

E. Design Implications

This MCP glove design has some inherent implications that may drive how the has layer may be integrated to form the complete Hybrid Spacesuit glove. The primary implications are:

1. **Bulkiness**: using a wetsuit neoprene fabric instead of a traditional textile, such spandex or cotton-based materials, makes the glove garment bulkier.

This may cause problems when integrating this layer not only with the other subsystems of the MCP layer, but also with the whole Hybrid Spacesuit glove system. Before sizing the GP layer, this thickness must be taken into account. This is one aspect the may affect the whole system, as it is considered, from Chapter 2 and 3, that the bulkier the garment, the less dexterous it is.

2. **Manufacturing Time Cost**: the way this MCP glove is manufactured currently can't be automated, since all elements are custom to the wearer. This makes the manufacturing time increased compared to other possible designs that incorporate sizing elements in a "one fits all" configuration. The software developed to create the ERL glove pattern helps to automate the process, but the hand sewing and gluing of the ERL subsystem as well as the molds needed to manufacture the PPD are time consuming. This drives the MCP glove development and motivates the use of the less complicated GP layer, since the MCP glove will always need to be custom.
3. **Thermal and Radiation Protection**: this MCP design focuses on trying to apply a uniform specific pressure all over the hand. However, the thermal and radiation protection have not been taking into account. This aspect will be integrated into the GP layer.
4. **Repair**: the MCP design doesn't anticipate field-repair needs if damaged. As this layer will be in the inner part the Hybrid Spacesuit glove, it is unlikely to be damaged. The GP layer is more likely to be affected by outside elements.

Therefore, this layer provides additional safely and protection by being a moderate pressure, should a rupture of the GP occur.

F. Pressure Assessment System

Attempts were made to develop a testing system that could objectively assess the distribution and amount of pressure that the different MCP glove configurations were able to apply.

The development of this system has not been successful yet. However, the work that was done around it is going be presented in Appendix 3, so all the information related to the work done can be accessible and considered as a reference for possible future work.

V. Conclusions

In this Chapter tools to build a low-pressure MCP garment were described to design baseline MCP for Hybrid Spacesuits. The different elements studied and developed are resources to be used in further MCP glove developments.

A library was created to store all the intrinsic stress-strain characteristics of different off-the-shelf fabrics that could be used in MCP garments. From these, a Wetsuit Neoprene (one side covered with spandex, thickness of 2.66 mm) was identified as a fabric that could be used to manufacture a MCP glove.

Following this finding, a software was developed using the fabrics' stress-strain properties from the library and a calculates for a specific pressure applied to the hand (2psi in our case). The output is the relation between the size that a circular garment

should have to apply the desired design pressure to a cylindrical body part. This information was then used to CAD a glove pattern highly personalized to any user.

The glove pattern was used to prototype a physical MCP glove. The design explored was comprised of three different layers (ERL, PPD, and AG). From iterating each element at least three times, different limitations and strengths from this MCP glove design were identified. The knowledge acquired during the iterative design process is then shared to the scientific community, so it will be easier in the future to continue iterating on this (or other) MCP glove patterns. To facilitate the development of other MCP gloves, as well as Hybrid ones, a list with all the problems and lessons learned during the MCP glove manufacturing are listed:

A. Elastic Restrain Layer

1. If a thread is used to create a strong bond between pieces of the pattern made from elastic fabrics, is better to use an elastic thread, i.e. polyester-based, than a strong and inelastic one, i.e. Kevlar, as the elasticity of the thread enables the surrounding fabric deal with less stress when being stretched, making the fabric to be less likely to tear apart.
2. The blind stitch seems to be the best kind of sewing technique for a MCP garment made of neoprene as it allows the inner face of the fabric to not have discontinuities due to thread presence, and still strongly bonding different fabric pieces.
3. The neoprene, by itself, doesn't allow a good implementation of a blind stitch seam, as its isotropic warp-less nature catastrophically reacts when it is

punctured. However, this can be addressed if the neoprene is covered by other thinner warp-based fabrics, such as spandex, as they interact better with stitches and help the neoprene to improve its structural integrity, avoiding it to be torn apart.

4. To fill any punctures or holes done on a neoprene fabric, an extremely neoprene-specific cement material must be used. In our case, it could be seen how a silicone-based resin, although being able to stick to the neoprene, quickly ripped off. It is better a neoprene specific product, as it is the neoprene cement. The properties of this product proved extremely useful when bonding neoprene.
5. The most problematic sites of the glove when bonding are those sites with sharp turns, such as the finger tips. Special attention must be given to these points, as they can cause structural instability to the whole garment.

B. Palmar Pressure Distributor

1. Silicone seems to be the perfect material for this scenario. However, something that may ensure a better stability of the system is the inclusion of a reinforcing elements inside of it. Like reinforced concrete, a couple metallic bars could be placed in the interior of the silicone, thus improving the strength and stability of the PPD system, and even helping it to be integrated with the other subsystems.
2. It is important to avoid discontinuities in the palmar side of the PPD, as they quickly create skin injuries and discomfort to the user. If molds are

being used, air bubbles may be present, so shakers or vacuums should be used to minimize their presence in the solutions being cured.

3. Mold should be prioritized to create the desired shape of the silicone, rather than trying to work on the silicone when it is already solid. Silicone, as it is quite flexible and elastic, is difficult to cut or modify when it is cured.

C. Anchoring Gauntlet

1. The inelastic synthetic restraints, along with Velcro, seems to be the best way to apply pressure over a whole area. The restraints helped anchor the whole system to a fixed point (the wrist) as well as to apply maximum pressure on the PPD. However, these inelastic bands are quite bulky, and the Velcro system doesn't allow the user to always apply the same pressure every time it is donned. This same problem would be encountered if laces were used. A system should be explored to ensure a uniform and continued pressure is applied over the hand, not only with respect to the other subsystems of the MCP glove, but with respect to the different times that the glove is donned.
2. A balance between number of elements on the system and functionality should be sought. It is true that each element incorporated may help achieve the design goals, but they also increase the possible failure points, increasing risk, and increasing volume thus reducing dexterity.
3. 3D printed elements are extremely useful for quick prototyping, but in rare cases they can be considered part of a final design. PLA, for example, is a

plastic highly dependent on temperature, so it could never be used as a part of a ready-to-flight garment.

4. The "click-and-go" mechanism not only helped maintain the ERL on its place between fingers when donned, but also made the glove easier to don and doff.

Future work includes evaluating the pressure applied and iterating on the glove to achieve the desired level of pressure. This work informs future Hybrid Spacesuit designs by providing an opportunity to investigate the primary considerations for a functional MCP garment.

Chapter 5

Conclusions

The objective of this final chapter is to give a general overview of the conclusions derived from all the work performed and state their relationship with the broad main objective of this Thesis.

The stated objective of this Master Thesis was to **perform an engineering analysis of the Hybrid Spacesuit concept**. This work was to serve as an initial investigation into the system architecture and serve as a baseline investigation of a hybrid spacesuit glove.

To ensure the objective was met, multiple contributions to Hybrid spacesuit design were presented in this Thesis:

1. A trade space analysis was performed to evaluate the most beneficial pressure contribution of the MCP and GP layers to the Hybrid Spacesuit system.
2. The relationship between gas pressure level and hand dexterity for the GP glove layer was investigated.
3. Different design tools were provided for MCP garment development, and a concept for the MCP glove layer was developed.

In Chapter 2, a spacesuit trade study methodology was established that can provide an unbiased evaluation of the Hybrid Spacesuit design. As the trade study depended on data from the literature, it can continue to be improved with additional

studies. For example, this thesis has already identified the need to change one of the parameters (Mobility) as the conclusions from Chapter 3. There remains, though a great degree of maneuvering across the architectures trade space of the Hybrid Spacesuits that can still be explored.

Also, by systematically exploring how the combination of a GP layer and a MCP layer would impact Mobility, Feasibility, Decompression Sickness prevention, Mass, Complexity, and Robustness, a broad view on how the hybrid double-pressure layer spacesuit configuration would change as compared to the current spacesuits, particularly when looking toward future planetary exploration missions.

Chapter 3 identified how a commercially manufactured pressurized glove could perform when used as the GP layer of a Hybrid Spacesuit. This glove is lighter, simpler and cheaper to manufacture than existing EVA gloves. It could be observed that by operating the gas-pressurized glove at lower pressures, it significantly improves the dexterity of its users: that relation followed a logarithmic relation. This gives support to the idea that by making the GP layer support smaller pressures dexterity can be quickly and greatly improved. As future work, the pressurized glove should be compared to EVA-rated glove. This would help to conclude which is the best kind of garment to be the GP layer of the Hybrid Spacesuit concept.

Finally, Chapter 4 was entirely dedicated to study the MCP layer of the Hybrid Spacesuit. This was done by developing a MCP glove pattern from the calculations of our custom software using data from our own created fabrics properties library. This chapter continued to evaluate the pattern and developing an MCP prototype glove.

After a great deal of iteration, a final design addressing many limitations of MCP garments was achieved. Although the last version was not yet a fully operable MCP glove at 2psi, the lessons learned regarding the prototype development also serves as a tool for future researchers to develop their own MCP garments.

With these three main contributions divided and shown in the different chapters of this Master Thesis, it can be stated that this Thesis was able to **perform an engineering analysis of the Hybrid Spacesuit concept**, through empirical and bibliographic studies, generating a baseline for future development of the Hybrid Spacesuit.

Bibliography

[1] K. Thomas and H. McMann, *US Spacesuits*. Chickester, UK: Springer-Praxis Publishing Ltd, 2006.

[2] D. A. Morgan, R. Wilmington, A. Pandya, J. Maida, and K. Demel, "Comparison of Extravehicular Mobility Unit (EMU) Suited and Unsuited Isolated Joint Strength Measurements," Johnson Space Center, Houston, TX, NASA/TP-1996-3613, 1996.

[3] D. . Williams and B. J. Johnson, "EMU Shoulder Injury Tiger Team Report," Houston, TX, NASA/TM—2003–212058, 2003.

[4] R. Scheuring *et al.*, "The Apollo Medical Operations Project: Recommendations to Improve Crew Health and Performance for Future Exploration Missions and Lunar Surface Operations," *Acta Astronaut.*, vol. 2008, no. 63, p. 8, Mar. 2008.

[5] S. Strauss, "Extravehicular Mobility Unit Training Suit Symptom Study Report," Johnson Space Center, Houston, TX, NASA/TP–2004–212075, 2004.

[6] A. Anderson and D. Newman, "Pressure Sensing for In-Suit Measurement of Space Suited Biomechanics," *J. Biomech.*, Submitted) In 2014.

[7] M. Gernhardt, J. Jones, R. Scheuring, A. Abercromby, J. Tuxhorn, and J. Norcross, "Risk of Compromised EVA Performance and Crew Health Due to Inadequate EVA Suit Systems," Human Research Program, Houston, TX, 2009.

[8] J. Norcross *et al.*, "Feasibility of Performing a Suited 10-km Ambulation on the Moon - Final Report of the EVA Walkback Test (EWT)," Johnson Space Center, Houston, TX, 2009.

[9] P. Webb and J. Annis, "Development of a Space Activity Suit." NASA, Nov-1971.

[10] J. M. Waldie, "Mechanical counter pressure space suits: advantages, limitations and concepts for martian exploration," *Mars Soc.*, pp. 1–16, 2005.

[11] D. J. Newman J. Hoffman, K. Bethke, C. Carr, N. Jordan, L. Sim, N. Campos, C. Conlee, B. Smith, J. Wilcox, G. Trotti, "Astronaut BioSuit System for Exploration Class Missions: NIAC Phase II Final Report," Massachusetts Instittute of Technology, Cambridge, MA, 2005.

[12] J. M. A. Waldie, "The Viability of Mechanical Counter Pressure Space Suit." MIT Department of Aeronautics and Astronautics and the Engineering Systems Division, Mar-2005.

[13] Z. L. Sim, "Design and Implementation of a Mechanical Counter Pressure Bio-Suit System for Planetary Exploration." MIT Department of Aeronautics and Astronautics and the Engineering Systems Division, 2006.

[14] R. Huerta, E. S. Kerr, and A. P. Anderson, "Mechanical Counterpressure and Gas-Pressurized Fusion Spacesuit Concept to Enable Martian Planetary Exploration," *48th Int. Conf. Environ. Syst.*, p. 15, Jul. 2018.

[15] F. A. Korona and D. L. Akin, "Evaluation of a Hybrid Elastic EVA Glove," 2002.

[16] S. Cruickshank and N. Hirschauer, "The alveolar gas equation," *Contin. Educ. Anaesth. Crit. Care Pain*, vol. 4, no. 1, pp. 24–27, Feb. 2004.

[17] R. R. Bishu and G. Klute, "The effects of extra vehicular activity (EVA) gloves on human performance," *Int. J. Ind. Ergon.*, vol. 16, no. 3, pp. 165–174, 1995.

[18] K. Tanaka, "Development and Evaluation of a Glove for Extravehicular Activity Space Suit without Prebreathing," *J. Ergon.*, vol. S2, no. 02, 2014.

[19] M. Mousavi *et al.*, "A new method of measuring the stiffness of astronauts' EVA gloves," *Acta Astronaut.*, vol. 97, pp. 130–137, Apr. 2014.

[20] K. Mitchell, A. Ross, R. Blanco, and A. Wood, "Hazard Analysis for Class III Space Suit Assembly (SSA) Used in 0ne-g Operations.pdf." NASA.

[21] J. Conkin, J. Norcross, and A. F. J. Abercromby, "Evidence Report: Risk of Decompression Sickness." NASA, 09-Jun-2016.

[22] A. F. J. Abercromby, J. Conkin, and M. L. Gernhardt, "Modeling a 15-min extravehicular activity prebreathe protocol using NASA's exploration atmosphere (56.5kPa/34% O2)," *Acta Astronaut.*, vol. 109, pp. 76–87, Apr. 2015.

[23] J. C. Buckey, *Space Physiology*. Oxford University Press, Inc., 2006.

[24] L. Vogt, J. Wenzel, A. I. Skoog, S. Luck, and B. Svensson, "European EVA decompression sickness risks," *Acta Astronaut.*, vol. 23, pp. 195–205, Jan. 1991.

[25] J. Norcross *et al.*, "Effects of the 8 psia / 32% O2 Atmosphere on the Human in the Spaceflight Environment," p. 72, 2013.

[26] ILC DOVER, INC, "Space Suit Evolution: From Custom Tailored To Off-The-Rack." 1994.

[27] T. C. Southern and N. A. Moiseev, "Novel Mechanical Counter Pressure Gloves." 47th International Conference on Environmental Systems, Jul-2017.

[28] Allison P. Anderson, "Addressing Design Challenges in Mechanical Counterpressure Spacesuit Design and Space-Inspired Informal Education

Policy." MIT Department of Aeronautics and Astronautics and the Engineering Systems Division, Feb-2011.

[29] J. M. A. Waldie, K. Tanaka, D. Tourbier, P. Webb, C. W. Jarvis, and A. R. Hargens, "Compression under a mechanical counter pressure space suit glove." J. Grav. Physiol., 2002.

[30] P. Webb, "The Space Activity Suit: An Elastic Leotard for Extravehicular Activity," *Aerosp. Med.*, vol. 8, 1968.

[31] P. Webb and J. Annis, "The Principle of the Space Activity Suit," *LR Cent. Natl. Aeronaut. Space Adm.*, no. 29, 1967.

[32] The MathWorks, Inc, *MATLAB and Statistics Toolbox R2017b*. Natick, Massachusetts (USA): The MathWorks, Inc.

[33] V. L. Alex, "Under the waves, above the clouds: A history of the pressure suit.," *Tech. Univ. Darmstadt*, p. 345, 2010.

[34] F. A. Korona, S. K. Walsh, and S. M. McFarland, "NASA EVA Glove Characterization Protocol Development," *48th Int. Conf. Environ. Syst.*, p. 20, Jul. 2018.

[35] F. F and E. E, "G*Power 3: A flexible statistical power analysis program for the social, behavioral, and biomedical sciences.," *Behav. Res. Methods*, vol. 39, pp. 175–191, 2007.

[36] T. M. Greiner, "Hand Anthropometry of U.S. Army Personnel," p. 428, Dec. 1991.

[37] D. J. Newman, “Astronaut Bio-suit System for Exploration Class Missions,” *NASA Inst. Adv. Concepts*, vol. Bimonthly Report, no. Phase II, Mar. 2005.

[38] L. Wang, “Study of Properties of Medical Compression Fabrics,” *J. Fiber Bioeng. Inform.*, vol. 4, no. 1, pp. 15–22, Jun. 2011.

[39] A. S. Iberall, “The Experimental Design of a Mobile Pressure Suit,” *J. Basic Eng.*, vol. 92, no. 2, p. 251, 1970.

[40] D. C. L. Judnick, “Modeling and testing of a mechanical counterpressure BioSuit system,” PhD Thesis, Massachusetts Institute of Technology, 2007.

[41] D. P. Gon and P. Paul, “Complex Garment Systems to Survive in Outer Space.” Journal of textile and Apparel, Technology and Management, Fall-2011.

[42] *SolidWorks*. Tennesse, USA: Dassault Systemes.

[43] T. Southern, D. P. Roberts, N. Moiseev, A. Ross, and J. H. Kim, “Space Suit Glove Design with Advanced Metacarpal Phalangeal Joints and Robotic Hand Evaluation,” *Aviat. Space Environ. Med.*, vol. 84, no. 6, pp. 633–638, Jun. 2013.

Appendix 1 – Fabrics Library

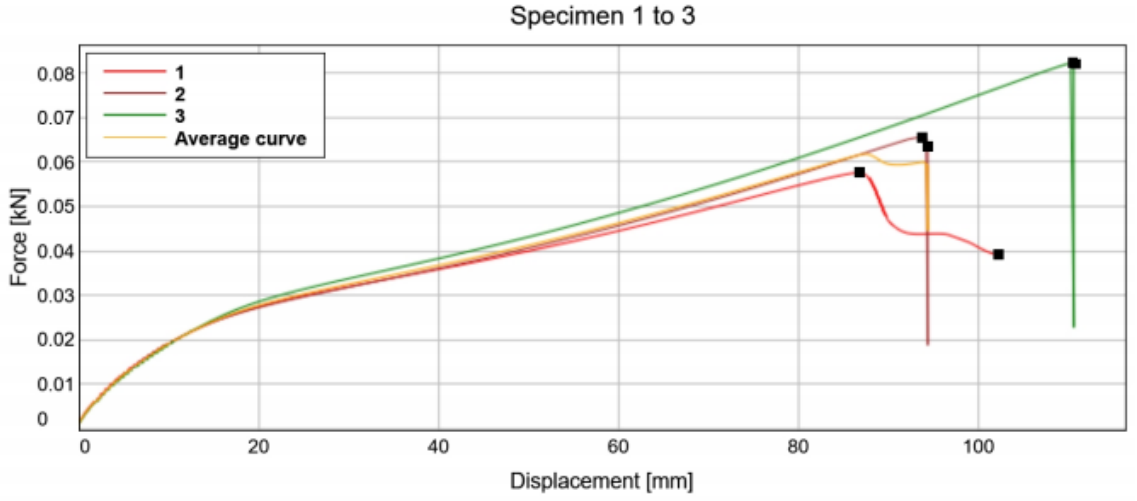

Figure A1.1. Neoprene Rubber. *Isotropic orientation. Thickness of 0.08 cm.*

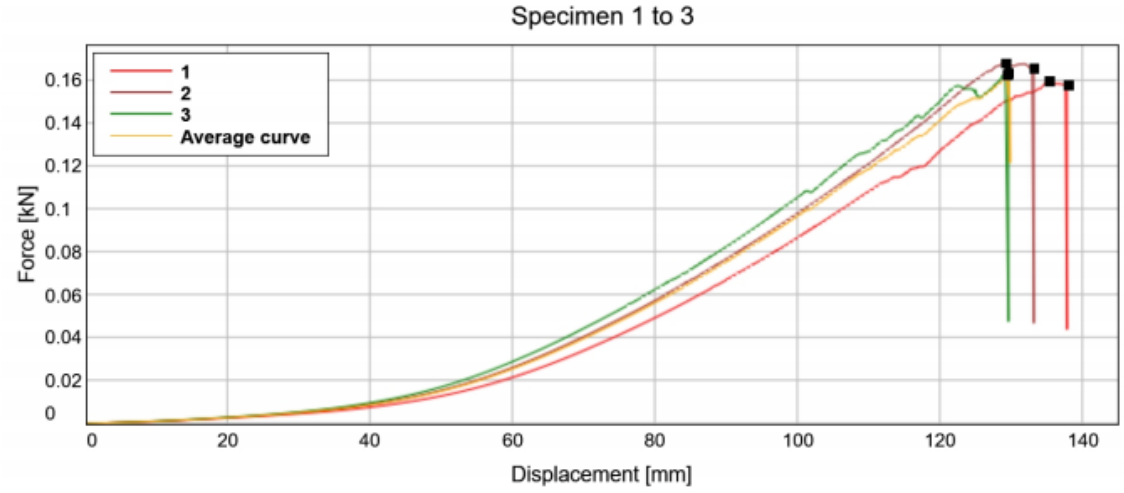

Figure A1.2. Suplex. *Warp orientation. Thickness of 0.066 cm.*

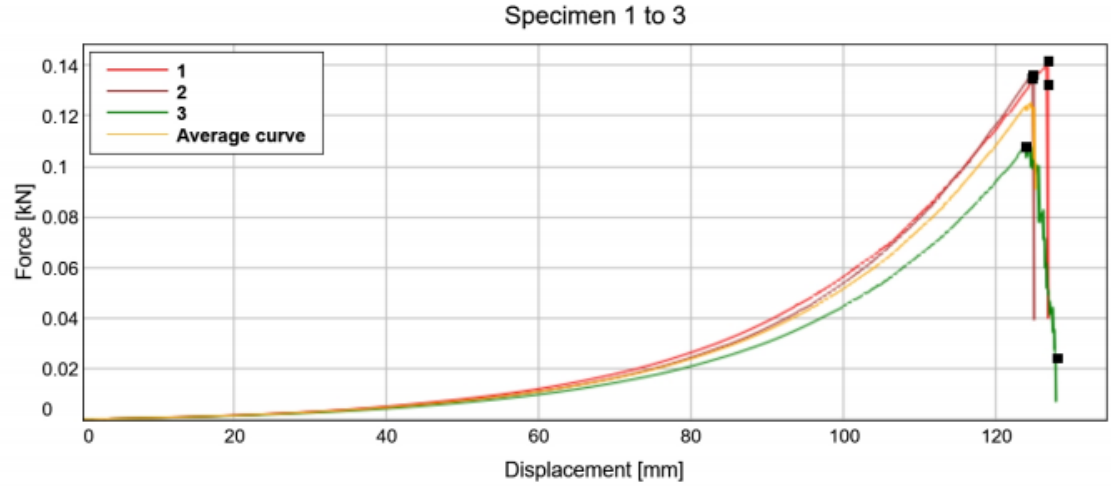

Figure A1.3. Cotton Lycra. *Warp orientation. Thickness of 0.064 cm.*

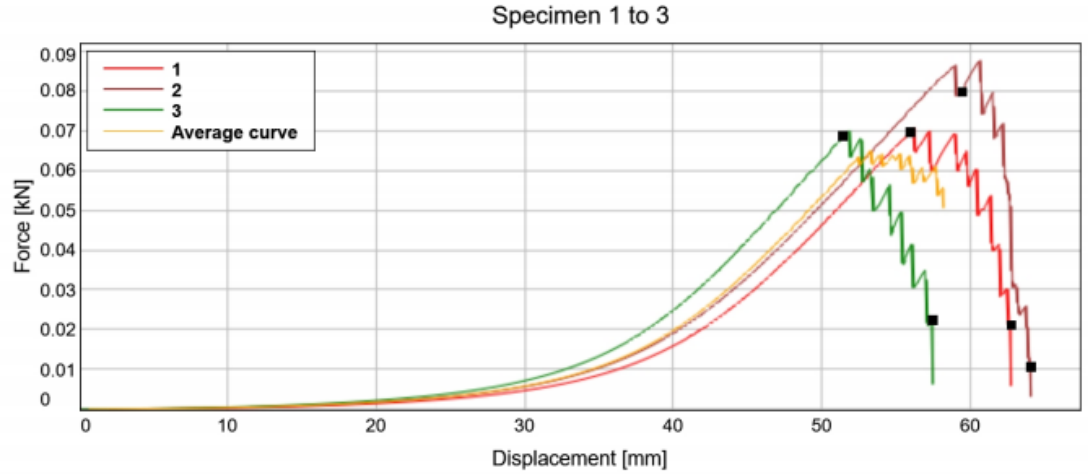

Figure A1.4. Rayon. *Warp orientation. Thickness of 0.04 cm.*

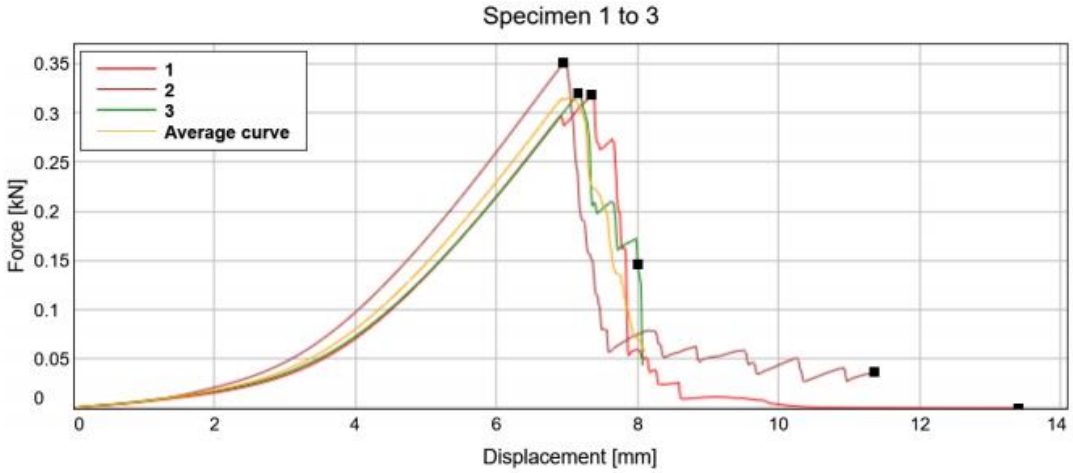

Figure A1.5. Cotton Heavy Duty Inelastic. *Isotropic orientation. Thickness of 0.051 cm.*

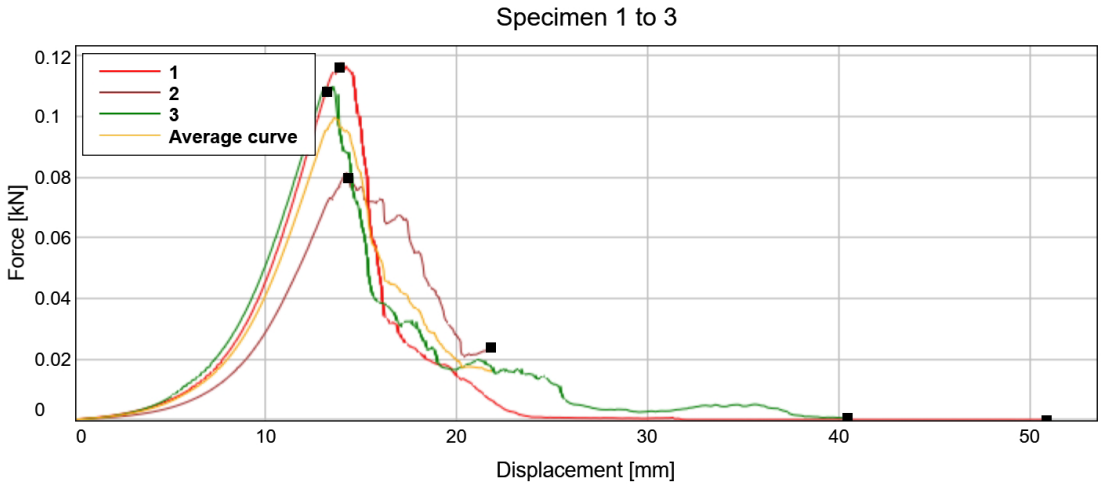

Figure A1.6. Cotton cozy flannel. *Isotropic orientation. Thickness of 0.15 cm.*

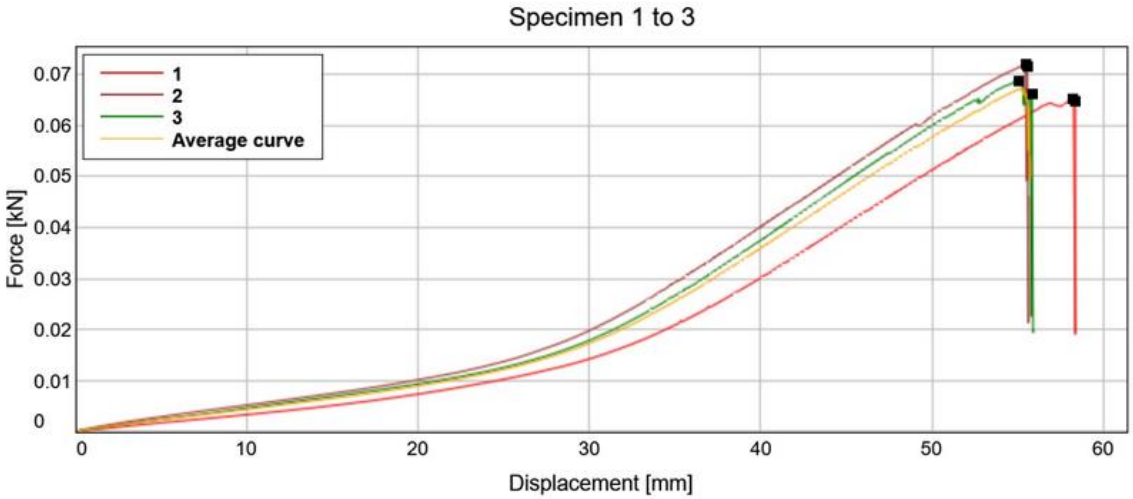

Figure A1.7. Foam-backed Headliner Fabric. *Isotropic orientation. Thickness of 0.5 cm.*

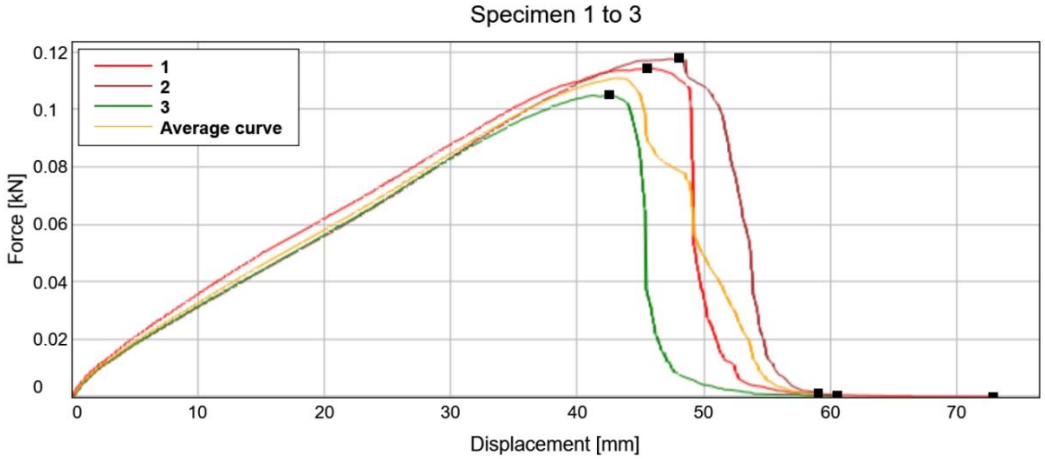

Figure A1.8. Vynil. *Isotropic orientation. Thickness of 0.02 cm.*

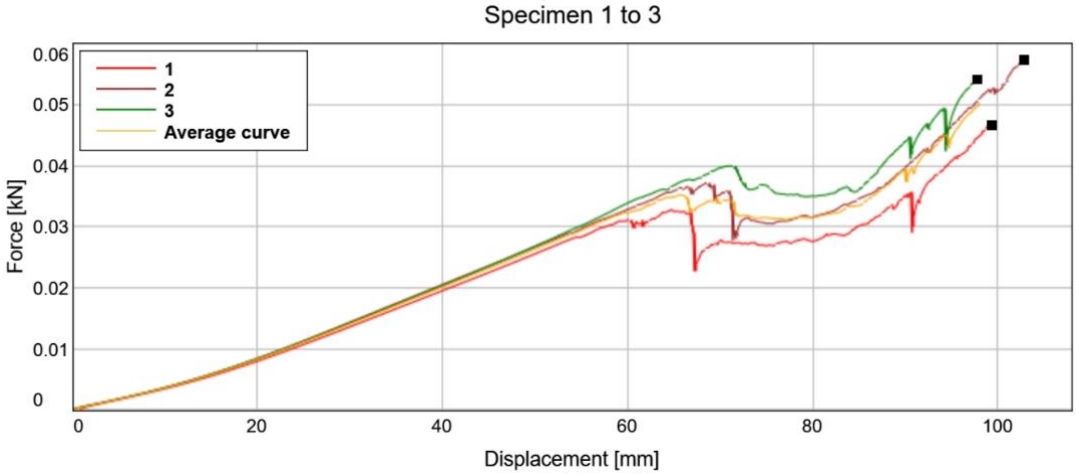

Figure A1.9. Wetsuit Neoprene. *Isotropic orientation. Thickness of 0.0266 cm.*

Appendix 2 – Pattern-Sizing MATLAB code

```
close all; clear all; clc;


pressure_required = 2*6894.76; %Pa


% thickness = 0.762 /1000; % mm -> m
thickness = 2.667/1000; % mm -> m

circumference_f = (.25:0.01:10) * 0.0254; % in -> m
radius_f = circumference_f/(2*pi);


stress_optimal = (pressure_required .* radius_f) ./ thickness;

% plot(radius_f,stress_required)

[p2, p3 thickness_stress_relation] = material_properties(6)


thickness = polyval(p3,stress_optimal);

figure
plot(stress_optimal,thickness)
title ('Stress Thickness Relation')
ylabel('Thickness (m)')
xlabel('Stress (Pa)')

stress_required = (pressure_required .* radius_f) ./ thickness;

strain_required = polyval(p2,stress_required)

figure
plot(radius_f,strain_required)
title ('radius strain relation')
xlabel('radius (m)')
ylabel('strain required')

circumference_initial = circumference_f./(1+strain_required);

plot(circumference_f/2*39.3701, circumference_initial/2*39.3701)
title('Half Circumference Function')
xlabel('Final Half Circumference')
ylabel('Initial required Half Circumference')

function [] = tension_finder(radius, thickness, width)
   radius
   thickness
   width
```

```
    tension = 1:1:100;
    stress = (tension./(thickness*width))

    pressure = (stress.*thickness)/(radius)

%     test_tension = [5.1 9.7 15.7 18 ]
%     test_resistance = [83815 29187 13100 12900]
    test_tension = [ 0 2.8 9.6 14 15.3 19  18 21.5 25] .* 4.44822;
%     test_pressure = [ 0.02 0.35 0.63 0.79 0.75 0.87 1.04 1.24 1.36] .* 6894.76;
    test_pressure = [0 34.12 61.42 77.02 73.12 84.82 101.39 120.89 132.59] .* 6894.76;

    figure
    hold on
    plot(tension,pressure)
    plot(test_tension, test_pressure)
    title('tension vs pressure')
    xlabel('tension (N)')
    ylabel('pressure (Pa)')

end


function [p2, p3, thickness_stress_relation] = material_properties(n)

    neo1 = importfile('C:\Users\Roger\Desktop\20181029_153328_1 (Neoprene_wetsuit 0.105)
(1).csv');
    neo2 = importfile('C:\Users\Roger\Desktop\20181029_153328_1 (Neoprene_wetsuit 0.105)
(2).csv');
    neo3 = importfile('C:\Users\Roger\Desktop\20181029_153328_1 (Neoprene_wetsuit 0.105)
(3).csv');
    bound = 4000;
    neo1(bound:end,:) = [];
    neo2(bound:end,:) = [];
    neo3(bound:end,:) = [];

    neo1{:,3} = neo1{:,3}.*1000;
    neo2{:,3} = neo2{:,3}*1000;
    neo3{:,3} = neo3{:,3}*1000;

    neodisp = horzcat(neo1{:,2}, neo2{:,2}, neo3{:,2});
    neoforce = horzcat(neo1{:,3}, neo2{:,3}, neo3{:,3});
    neostress = horzcat(neo1{:,4}, neo2{:,4}, neo3{:,4});

    neo_disp = mean(neodisp,2);
    neo_force = mean(neoforce,2);
    neo_stress = mean(neostress,2)*1000000;

    L_0 = 2 * 25.4;
    neo_strain = (neo_disp./L_0);

    poisson = 0.5

    width = 1 * 0.0254; % in -> m
```

```
    t_o  = 2.667/1000;
    thickness_stress_relation = t_o - t_o.* (neo_strain.*poisson)

    p1 = polyfit(neo_disp(1:end,:),neo_force(1:end,:), 1);

    p2 = polyfit(neo_stress(1:end,:),neo_strain(1:end,:), n); %This gives the aproximation of the strain
stress curve
% %     p3 = polyfit(neo_strain(1:end,:), neo_stress(1:end,:), n);

    p3 = polyfit(neo_stress(1:end,:), thickness_stress_relation,n)

    x = [0:100:400000];
    y = polyval(p2,x);


    figure
    hold on
%     plot(neo1{:,2}, neo1{:,3})
%     plot(neo2{:,2}, neo2{:,3})
%     plot(neo3{:,2}, neo3{:,3})
    plot(neo_disp, neo_force, '-')
    title('Displacement vs Force')
    xlabel('Displacement (mm)')
    ylabel('Force (N)')


    figure
    hold on
    plot (neo_strain, neo_stress)
    plot(y,x)
    title('Stress Strain')
    xlabel('Strain')
    ylabel('Effective Stress (Pa)')


end



function Untitled = importfile(filename, startRow, endRow)
%IMPORTFILE Import numeric data from a text file as a matrix.
%   UNTITLED = IMPORTFILE(FILENAME) Reads data from text file FILENAME for
%   the default selection.
%
%   UNTITLED = IMPORTFILE(FILENAME, STARTROW, ENDROW) Reads data from rows
%   STARTROW through ENDROW of text file FILENAME.
%
% Example:
%   Untitled = importfile('20181019_105512_1 (0.03 Neoprene Isotropic).csv', 2, 7669);
%
%    See also TEXTSCAN.

% Auto-generated by MATLAB on 2018/10/21 10:48:30
```

```
%% Initialize variables.
delimiter = ',';
if nargin<=2
    startRow = 2;
    endRow = inf;
end

%% Format for each line of text:
%   column1: double (%f)
%  column2: double (%f)
%   column3: double (%f)
%  column4: double (%f)
% For more information, see the TEXTSCAN documentation.
formatSpec = '%f%f%f%f%[^\n\r]';

%% Open the text file.
fileID = fopen(filename,'r');

%% Read columns of data according to the format.
% This call is based on the structure of the file used to generate this
% code. If an error occurs for a different file, try regenerating the code
% from the Import Tool.
dataArray = textscan(fileID, formatSpec, endRow(1)-startRow(1)+1, 'Delimiter', delimiter,
'TextType', 'string', 'EmptyValue', NaN, 'HeaderLines', startRow(1)-1, 'ReturnOnError', false,
'EndOfLine', '\r\n');
for block=2:length(startRow)
    frewind(fileID);
    dataArrayBlock = textscan(fileID, formatSpec, endRow(block)-startRow(block)+1, 'Delimiter',
delimiter, 'TextType', 'string', 'EmptyValue', NaN, 'HeaderLines', startRow(block)-1,
'ReturnOnError', false, 'EndOfLine', '\r\n');
    for col=1:length(dataArray)
        dataArray{col} = [dataArray{col};dataArrayBlock{col}];
    end
end

%% Close the text file.
fclose(fileID);

%% Post processing for unimportable data.
% No unimportable data rules were applied during the import, so no post
% processing code is included. To generate code which works for
% unimportable data, select unimportable cells in a file and regenerate the
% script.

%% Create output variable
Untitled = table(dataArray{1:end-1}, 'VariableNames',
{'Times','Displacementmm','ForcekN','TensilestressMPa'});


end
```

Appendix 3 – Pressure Assessment System

A. Introduction

The architecture for a testing system should be a static one: a mannequin-style hand that has pressure sensors embedded on its surface.

For anatomical accuracy, the hand, in its natural resting position, was 3D printed. Then, its surface was carved, and the sensors were permanently positioned so they didn't alter the smoothness and curvatures of the hand. The sensors that were used are Force Sensitive Resistors (FSR), because of their availability and easy implementation in small electronic systems. For data processing, an Arduino UNO was chosen.

This system contrasts with other ones that have been used, such as the one that Final Frontier Design implemented to study its MCP glove performance[27]: it was a glove that had FSR sensors, so the subject testing the MCP glove had to wear the sensing one under it. Two main flaws were detected on that configuration:

1. The sensing glove was adding a non-anatomical volume to the system. That would alter the results, because the MCP glove wouldn't be applying its pressure directly to the skin, but to a bulkier not-real dimensioned hand.
2. The pressure sensors that were being used, Force Sensitive Resistors, are quite unreliable in dynamic conditions, because the values that they give change if they are bended or not.

So, having a static evaluation system could solve those problems. However, the fact that the gloves then could be tested just in a single position, and thus not being able

to see how the pressure distribution changes when the MCP gloves are being actively used by a subject, became a concern. The definitive decision was that it would be preferable to have limited, but truly reliable, data.

B. Hand Support

To end up with a 3D printed anatomically-sized hand, a specific path must be followed. For 3D printing, a 3D computerized model needs to be done. An easy way to model it is by scanning a real hand. As to scan an object you need it to be stable and fixed to a support, a real hand can't be used: instead, a sculpture of the hand can be manufactured through a mold of the original hand.

i. Plaster Mold

To create the mold of a human hand, a silicone material was used: called Elite Double 32 from Zhermack with a 32 shore A, which is sold as a base and a catalyst with a working time of 10 min and a setting time of 20 min. A cardboard box lined with plastic was partially filled, and the hand was placed in it for 30 minutes (Figure A3.1a). After that, thanks to the elasticity of the mold, the hand was pulled out without breaking the mold. The silicone mold was left 24 hours to dry and finish the curing process. Once it was completely solidified, the mold was filled with a plaster liquid mixture. The plaster remained inside of it for 48 hours. After that time, the mold was cut down and the plaster hand was liberated. Due to the high amount of force used to cut the mold, the fingers of the plaster hand broke (Figure A3.1b). The fingers were glued back (Figure A3.1c), but some holes on the plaster couldn't be

filled. This issue would later be solved through software during the 3D scanning process.

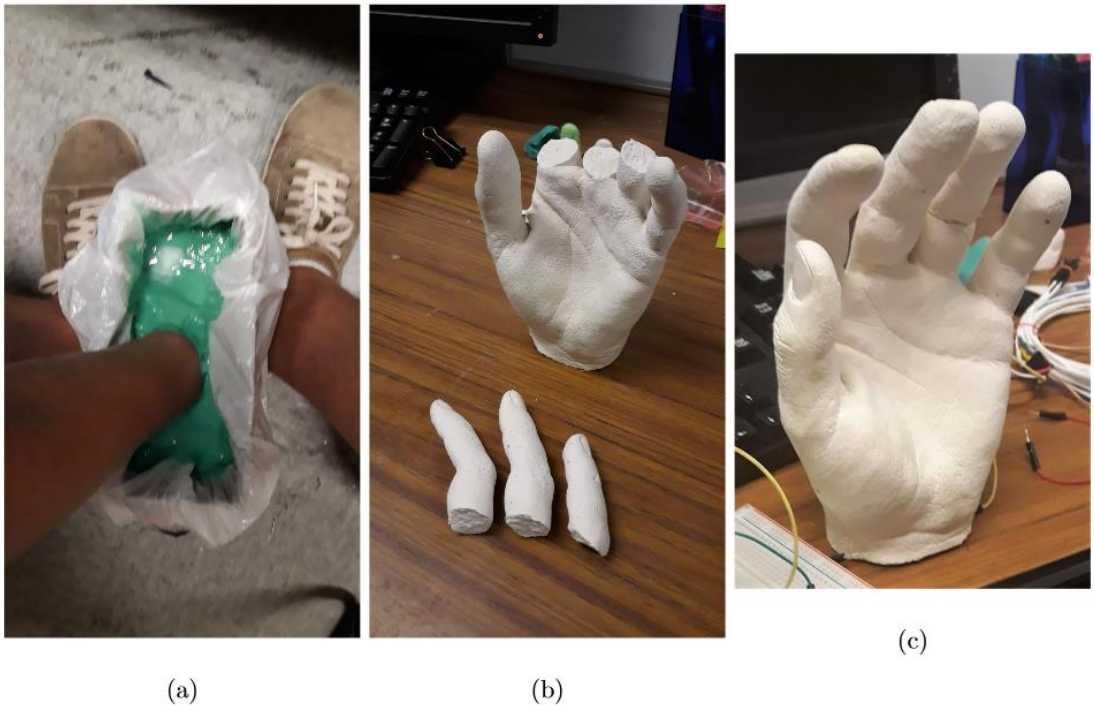

(a) (b) (c)

Figure A3.1. The process of how to develop a plaster hand anatomically exact to a real human one is depicted. *(a) Creation of the silicone mold; (b) Broken plaster hand after removing it from the silicone mold; (c) Final resulting plaster hand mounted and ready to be scanned*.

ii. Computerized Model

The plaster hand was scanned with a NextEngine HD desktop 3D Scanner in the ITLL facilities at the University of Colorado Boulder and a 3D document was created. The scan, however needed some editing: not only were there visible holes and imperfections of the plaster hand, but also some discontinuities appeared in the generated grid (Figure A3.2-left). To clean and make the grid smoother, an open source 3D scanned hand was downloaded and was then combined with the grid resulting from the previous scanning using the MeshMixer and Blender software (Figure A3.2-right). This processing switched the hand, becoming a right hand. Also,

a standing platform and cylinder simulating the most distal part of the arm were implemented for structure and stability purposes (Figure A3.3).

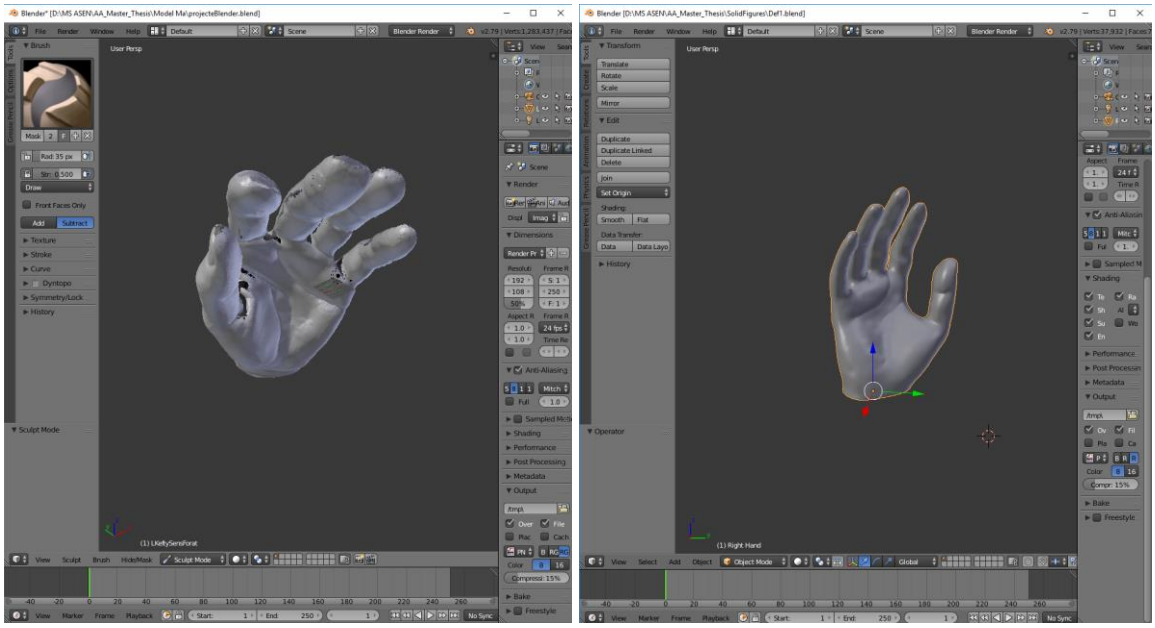

Figure A3.2. 3D Hand Scan Cleaning. *These pictures show the process of cleaning the 3D scan performed on the plaster hand. In the left picture it can be easily seen the defects and discontinuities on the hand surface. After cleaning it and mixing the hand grids, a clean hand surface can be seen in the right figure.*

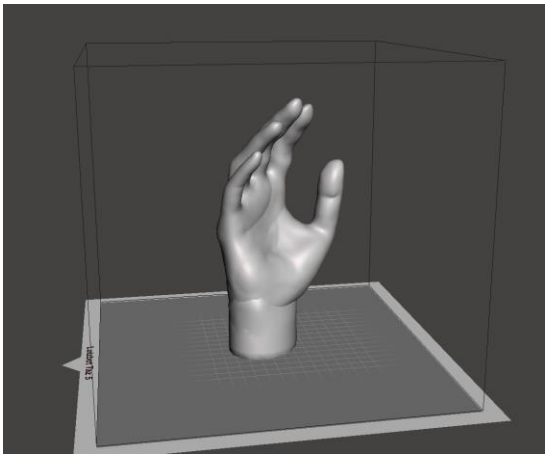

Figure A3.3. 3D Hand Computer Model. *Final 3D hand model smoothed and cleaned that will be printed and will be used as the support for the MCP gloves pressure testing system*

iii. 3D Print

The hand was 3D printed with PLA using a LulzBot TAZ6 printer located in the ITLL of the University of Colorado Boulder. The wall thickness was selected to be 5mm., allowing it to be able to carve the surface without having to worry about possible structure collapse. After a 26-hour printing, the hand support was taken out from the printer and it was smoothed. First, a heat bath was applied to it with a heat pistol, and, then, the surface and irregularities of the surface of the hand were sanded. The resulting 3D printed hand support can be seen in Figure A3.4.

Figure A3.4. 3D Printed Hand Support. *Finished 3D printed Hand support which, although being sanded, still shows some discontinuities over its surface due to the 3D printing technique used. However, the surface is smooth enough so that these discontinuities won't have any effect on the donning/doffing of the glove nor on the applied pressure sensing.*

C. Pressure Sensors

The Force Sensitive Resistors (FSRs) are widely used for DIY electronics, due to their cheap price and their size. However, this comes with a handicap: the variability of values between the same model sensors is strongly variable, and they are really susceptible to bending due to their architecture. So, each one of the sensors must

undertake a calibration process before they can be implemented in the printed plastic hand.

i. Working Theoretical Method

FSR consists of three main layers, as it can be seen in Figure A3.5. Two of those are able to pass current through them if they are in contact, and the third, the one in the middle of those, is the spacer, which separates the two conductive layers. As more physical pressure is applied (squeezing, weight…) the higher the amount of current that can pass through it. Or in other words: the resistance (R) decreases when the force is applied over its surface.

The model used is the Interlink Electronics FSR TM 400, which has a 4mm diameter active sensing area. When maximum pressure is being applied to them, their resistance is equal to 2.5kOhms, more or less.

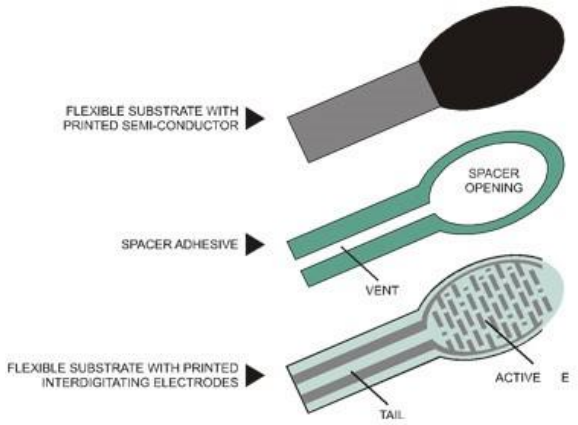

Figure A3.5. FSR Architecture. *Force Sensitive Resistor explosion view of its architecture. Diagram from Adafruit (learn.adafruit.com).*

ii. Calibration Setup

As previously stated, FSR sensors need to be calibrated so that the variance shown between them is corrected. In order to do so, a calibration system was built so all

pressure values could be corrected for each of the sensors. With that, all the pressures detected by the different sensors would be then comparable and empirically correct. The calibration setup can be seen in Figure A3.6. It consists of:

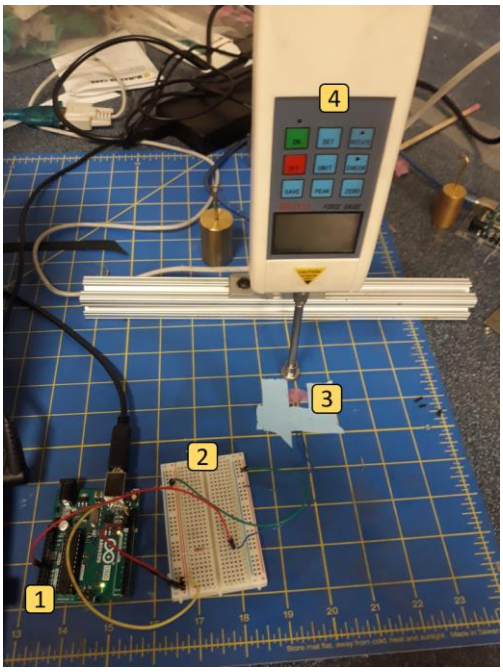

Figure A3.6. FSR Calibration Setup. *General overview of the of the FSR calibration setup.*

1. **Arduino UNO:** the shield provides a constant DC current of 5V, and reads the voltage levels coming out of the measured FSR sensor. With that values, and after being precisely programmed, it acquires the real resistance levels of the FSR through time.
2. **Voltage Divider:** using a known 10kOhm (+/-5%) resistor measured in each case with a multimeter, the voltage divider is implemented to enhance the voltage signal coming from the FSR sensor. This allows us to discover the unknown FSR resistance using the following Equation A3.1:

$$R_1 = \frac{R_2 \cdot V_{in}}{V_{out}} - R_2 \qquad \text{(A3.1)}$$

3. **FSR Sensor:** there are a total of 7 different FSR sensors.
4. **Force Gauge:** the force gauge is used to record the dynamic force that is being applied to the FSR sensor. At the tip it has an extremely thin silicone membrane so that it can apply uniform force on the sensor surface. The force gauge is connected to the computer and provides, through a serial port, the force values in Newtons. To facilitate its operation, a small support and slider were implemented.

iii. FSRs Calibration

The protocol repeated through all the FSR sensors was the following:

1. The voltage divider is implemented in the motherboard, previously checking the exact value of the resistance with a multimeter. The FSR is connected to the motherboard as well and the system is properly wired to the Arduino UNO.
2. An extremely thin silicone layer is placed over the FSR and both of them are fixed together over the surface, to avoid noise due to movement and to be able to precisely repeat the same movements throughout.
3. The force gauge is placed over the FSR sensor, so the rounded tip is perfectly pressing it with its weight.
4. The Arduino UNO and the Force Gauge are switched on.

5. The recording program is started so the values of the FSR resistance are recorded through the Arduino and the force is recorded through the force gauge simultaneously.
6. The force gauge is elevated 4 times, so the dynamic pressure being applied is recorded.
7. The recording program is then closed, and the data is stored in a txt file in the computer.
8. This process (from 3 to 7) is repeated.
9. The calibration program is run with both of the data sets:
    a. The two data sets (Resistance and Applied Pressure) are synched knowing that the last time recorded is the same one in both of them. The difference between these times is calculated and corrected in one of the data sets.
    b. As the average of values recorded is bigger than 5000 per data set, a decimation factor was implemented to decrease the calculation times. This allows the user to just work with 1 out of X (desired number) values of each data set.
    c. Now, for each pressure value its time associated is searched in the resistance data set. When found, that resistance is appended in a new dictionary with the correspondent pressure. This is done to all the values.

d. The correlation between recorded applied pressure with recorded resistance is then plotted as shown in Figure A3.7.

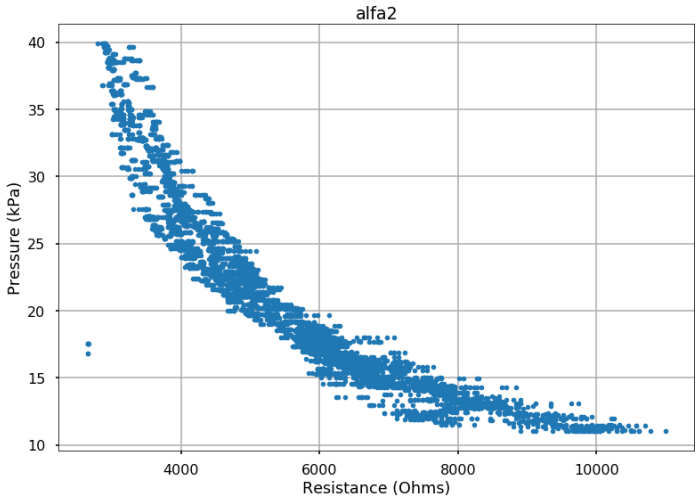

Figure A3.7. Example of Calibration Plot Unfitted. *Example of the collected data from an FSR sensor (Alfa) before fitting its calibration curve*

e. The calibration program then fits an exponential curve over the data in dark blue (Figure A3.8). The exponential curve, through literature and empirically testing, was found to be the best fitting type of curve.

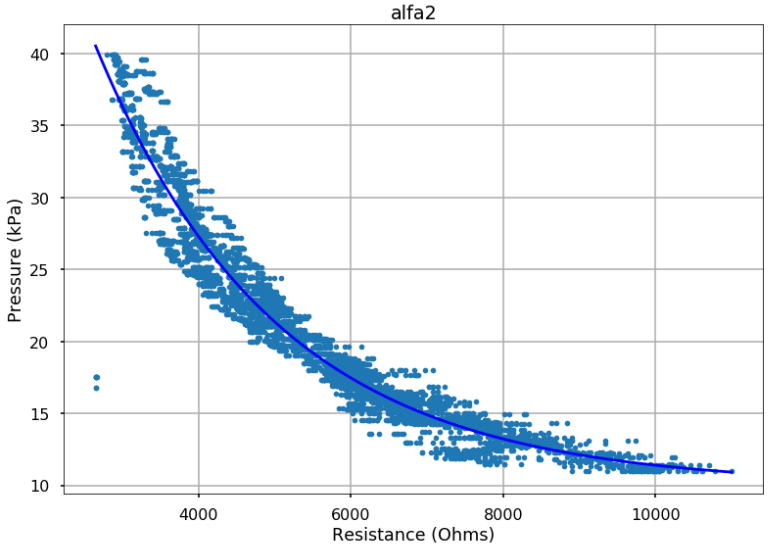

Figure A3.8. Example of Calibration Plot with its Curve Fitted. *Example of the collected data from an FSR sensor (Alfa) after fitting its calibration curve.*

f. The fitted curve is then recorded and will be used, afterwards, as the curve to be used to check the pressure in the final glove pressure analysis architecture.

iv. Glove Box Interaction

As the MCP glove will be tested inside a glovebox to simulate specific environmental pressure conditions, it was checked if the low pressures created in the glovebox had any effect on the FSR sensors. FSR are pressure sensors, but, theoretically, they only change their resistance properties when they face an increment of pressure due to contact forces. So, what was expected is to out find that there would be no noticeable effects on the FSRs.

To check that, an FSR sensor was connected directly to a multimeter, and both of them were placed in an easy to view place inside the glovebox (Figure A3.9). Then, the pressure inside the glovebox was progressively lowered to 3.2psi.

Figure A3.9. FSR Test Inside the Glovebox. *The multimeter (green, front) connected to the FSR sensor (blue wires, front) displays a 0 value inside the glovebox, while the pressure reader (orange, back) shows that the glovebox has a 3.2psi environmental pressure*

As was expected, no variance in the FSR sensor resistance was found during all the process, so it could be concluded that there would not be any noticeable effect due to that when FSRs were used inside the glovebox in the future.

D. Final Set Up

Once the different elements were ready, the FSR sensors and the Hand base, the last thing to be done was to build the static hand pressure recorder system. In order to do so, first, the hand was mapped to identify the most valuable locations of the FSR sensors and their wires on the surface of the hand, then the system was embedded on the surface, fixed and sanded, and finally, the FSRs were connected to the Arduino UNO and the computer.

i. Mapping

Initially, to identify the most valuable points where to set up the FSRs, a literature review was performed to find similar experiments that also faced this issue [27], [40]. Up to 30 locations were identified and marked over the surface of the 3D computer hand model (Figure A3.10). From all these locations, a total of 5 were selected as representative of the other ones. Those chosen are, in order:

1. In the middle of the middle finger in the anterior part.
2. In the middle of the left side of the thumb.
3. In the middle of the concavity of the palm, in the anterior part of the hand.
4. In a side of the anterior part of the hand, under the little finger, and
5. In the farthest part of the palm's concavity.

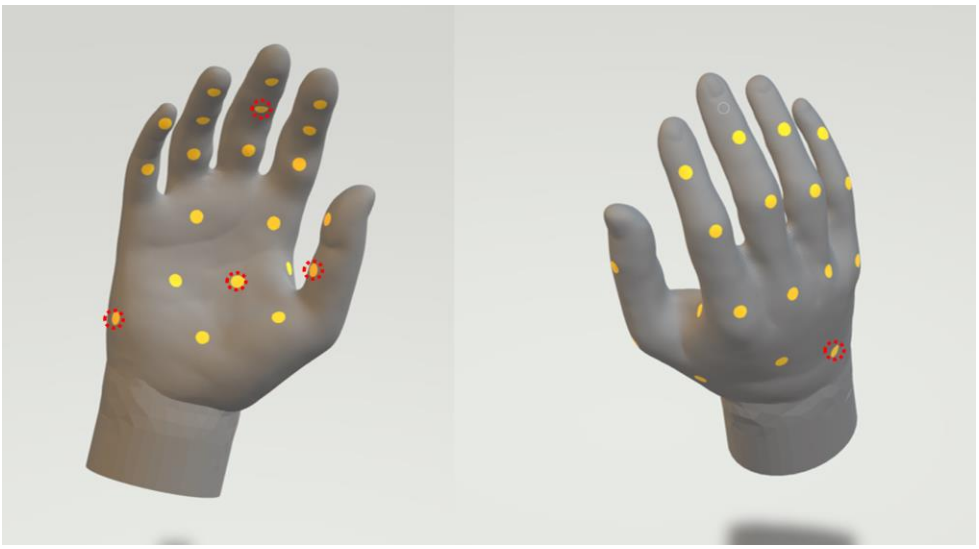

Figure A3.10. SR Placements on a 3D Computerized Hand Model. *Back (right) and frontal (left) view of the 3D computerized hand model with the identified FSR sensors locations painted as yellow dots. Highlighted in red, the 5 selected locations.*

ii. Failure Stopping Point

After all the work done on the topic, it had to be stopped before being able to be proved. This was due to the fact that when some FSR sensors were embedded to the 3D printed hand, they broke, and in the ones that did not break, the information displayed was not considered reliable enough.

Due to time constraints, the Testing Workbench could not be successfully finished and implemented.

However, the system architecture, considering all its elements, may be successful after more iterations, and could even be used in a future Hybrid Spacesuit project.